Published in final edited form as:

Reproduction. 2016 September ; 152(3): 245–260. doi:10.1530/REP-16-0129.

Reproductive age-associated fibrosis in the stroma of the mammalian ovary

Shawn M. Briley[#1], **Susmita Jasti**[#1], **Jennifer M. McCracken**[2], **Jessica E. Hornick**[3], **Barbara Fegley**[1,4], **Michele T. Pritchard**[2], and **Francesca E. Duncan**[1,§]

[1]Department of Anatomy and Cell Biology, University of Kansas Medical Center, Kansas City, KS 66160

[2]Department of Pharmacology, Toxicology, and Therapeutics, University of Kansas Medical Center, Kansas City, KS, 66160

[3]Biological Imaging Facility, Northwestern University, Evanston, IL 60208

[4]Electron Microscopy Research Laboratory, University of Kansas Medical Center, Kansas City, KS 66160

[#] These authors contributed equally to this work.

Abstract

Under normal physiological conditions, tissue remodeling in response to injury leads to tissue regeneration without permanent damage. However, if homeostasis between synthesis and degradation of extracellular matrix (ECM) components is altered, fibrosis – or the excess accumulation of ECM – can disrupt tissue architecture and function. Several organs, including the heart, lung, and kidney, exhibit age-associated fibrosis. Here we investigated whether fibrosis underlies aging in the ovary - an organ that ages chronologically before other organs. We used Picrosirius Red (PSR), a connective tissue stain specific for collagen I and III fibers, to evaluate ovarian fibrosis. Using brightfield, epifluorescence, confocal, and polarized light microscopy, we validated the specific staining of highly ordered PSR-stained fibers in the ovary. We next examined ovarian PSR staining in two mouse strains (CD1 and CB6F1) across an aging continuum and found that PSR staining was minimal in ovaries from reproductively young adult animals, increased in distinct foci in animals of mid-to-advanced reproductive age, and was prominent throughout the stroma of the oldest animals. Consistent with fibrosis, there was a reproductive aged-associated increase in ovarian hydroxyproline content. We also observed a unique population of multinucleated macrophage giant cells, which are associated with chronic inflammation, within the ovarian stroma exclusively in reproductively old mice. In fact, several genes central to inflammation had significantly higher levels of expression in ovaries from reproductively old mice relative to young. These results establish fibrosis as an early hallmark of the aging ovarian stroma, and this altered microenvironment may contribute to the age-associated decline in gamete quality.

[§]Corresponding Author: fduncan@kumc.edu.

Declaration of interest

The authors have no conflicts of interest.

Keywords

inflammation; macrophages; giant cells

Introduction

The female reproductive system is the first organ system to show overt signs of physiologic aging in the human and is characterized by a marked reduction in both gamete quantity and quality beginning when women reach their mid-thirties -- a phenomenon referred to as the maternal age effect (Broekmans, et al. 2009). Reproductive aging is associated with aneuploidy, miscarriages, birth defects, and infertility, and such consequences are a significant societal concern as more women globally are delaying childbearing (Heffner 2004, Johnson, et al. 2012, Nagaoka, et al. 2012). Although all women experience reproductive aging, the mechanisms underlying this phenomenon are not fully elucidated.

Data from Assisted Reproduction Technologies (ART) demonstrate that the age-associated decline in fertility is primarily attributable to defects at the level of the gamete. For example, when women of advanced reproductive age conceive using donor oocytes from young individuals, live birth outcomes reflect the age of the donor (Check, et al. 2011). In effect, donor oocytes from young women rescue the maternal age effect. Whether the maternal age effect is due to gamete intrinsic or extrinsic factors, or a combination of both, is unknown. Oocytes do not develop in isolation but rather they are surrounded by companion somatic cells within the context of ovarian follicles which themselves develop within and depend upon a complex stromal microenvironment. The ovarian milieu is composed of a structural network of extracellular matrix (ECM) components and a heterogeneous array of fibroblasts, smooth muscle cells, endothelial cells, theca-interstitial cells, and immune cells. This ovarian microenvironment can have a significant impact on follicle and oocyte quality. For example, using a mouse model of reproductive aging, it has been shown previously that secondary follicles isolated from reproductively old mice have altered growth and survival, hormone production profiles, and gamete quality outcomes when grown *in vitro* relative to follicles isolated from young mice (Hirshfeld-Cytron, et al. 2011). These results suggest that there are inherent differences between these follicle cohorts that may arise from the distinct ovarian microenvironments from which they were derived. Thus, understanding how the ovarian stroma changes with advanced reproductive age is of critical importance for better understanding the decline in gamete quality. Of note, it was documented that ovaries from reproductively old mice were more rigid compared to those from reproductively young mice, suggesting the presence of age-associated fibrosis (Hirshfeld-Cytron, et al. 2011).

Fibrosis is due to an excessive amount of ECM that replaces parenchymal tissue. ECM is composed of collagens, elastin, glycoproteins, and proteoglycans, which comprise connective tissue and basement membranes. Collagen is the main structural protein family of connective tissue and provides structural integrity to tissues in addition to regulating their function through signaling. Changes in the collagen matrix of soft tissues mostly affect the fibrillar type I and III collagens, and type I collagen is the most ubiquitously expressed ECM molecule within the mouse ovary (Alves, et al. 2015, Berkholtz, et al. 2006). Fibrosis occurs

when normal tissue remodeling and wound-healing responses are not properly regulated; this can lead to aberrant tissue architecture and thereby compromised organ function (Wynn and Ramalingam 2012). Inflammation also plays a fundamental role in fibrosis (Libby 2007, Sziksz, et al. 2015). There are several organ systems that become fibrotic with age. For example, collagen accumulates with age in the heart, which leads to fibrosis and contributes to diastolic dysfunction (Horn and Trafford 2015). In the lung, aging is associated with an increase of chronic lung diseases associated with fibrosis such as idiopathic pulmonary fibrosis and chronic obstructive pulmonary disease (Kapetanaki, et al. 2013). In the aging kidney, glomerulosclerosis and interstitial fibrosis results in a decreased glomerular filtration rate (Denic, et al. 2016, Sangaralingham, et al. 2016). Whether fibrotic changes occur in the mammalian ovary, which ages up to decades prior to other organs in humans, has not been systematically investigated.

Here we characterized and applied Picrosirius Red (PSR) staining to assess ovarian fibrosis during physiologic reproductive aging in two mouse strains. PSR is one of the most important selective histological stains used to study fibrillar collagen networks in tissue sections and is frequently used to evaluate fibrosis (Coleman 2011, Junqueira, et al. 1979, Lattouf, et al. 2014, Montes and Junqueira 1991). PSR is an anionic dye comprised of six sulfonate groups that can associate along cationic collagen fibers (Coleman 2011, Lattouf, et al. 2014). This dye specifically binds to collagen I and III fibrils and is thought to detect more advanced stages of fibrosis (Coleman 2011, Lattouf, et al. 2014). We evaluated PSR staining in fixed paraffin-embedded ovarian tissue sections using four imaging approaches, including brightfield, epifluorescence, confocal, and polarized light microscopy, which together demonstrate the specificity and versatility of this stain. We then demonstrated that during reproductive aging, PSR staining begins as discrete foci that expand throughout the ovarian stroma coincident with increased hydroxyproline levels, the presence of multinucleated macrophage giant cells, and increased expression of genes involved in inflammation. Taken together, this study provides definitive evidence at the histological, biochemical, and gene expression levels of prominent age-associated ovarian fibrosis.

Materials and Methods

Animals and ovarian and liver tissue samples

Ovarian tissue was harvested from two mouse strains (CD1 and CB6F1), which exhibit reproductive aging phenotypes including increased egg aneuploidy (Chiang, et al. 2010, Hornick, et al. 2015, Merriman, et al. 2012, Treff, et al. 2016). Reproductively young CB6F1 mice (6-12 week old) were obtained from Envigo (Indianapolis, IN), and reproductively old CB6F1 mice (14-17 month old) were obtained from the National Institutes on Aging Aged Rodent Colony (National Institutes of Health, Bethesda, MD). For this strain, these two age cohorts are herein referred to as reproductively “young” and “old,” respectively. For each experiment, ovarian tissue from a minimum of 3 animals per age group was examined and representative images are shown. Liver tissue from mice exposed to chronic carbon tetrachloride (CCl_4) to induce fibrosis was used for validation purposes, and these mice were generated as previously described. (Constandinou, et al. 2005, Pritchard and Nagy 2010, Weber, et al. 2003). All mice were housed in a controlled barrier facility at

the University of Kansas Medical Center's (KUMC) Research Support Facility under constant temperature, humidity, and light (12h light/12h dark). Food and water were provided *ad libitum*.

CD1 mice (Envigo) were bred at the Northwestern University and euthanized at various ages ranging from 6 weeks to 22 months. Histological ovarian sections from this aging continuum were a generous gift of Dr. Teresa K. Woodruff (Northwestern University). For this strain, the specific animal age used for each experiment is denoted throughout the text. All animal experiments described here were approved by the Institutional Animal Care and Use Committee (KUMC or Northwestern University) and were in accordance with National Institutes of Health Guidelines.

Tissue processing

Tissue samples were fixed in either 10% Formalin (liver) or Modified Davidson's (ovary) (Electron Microscopy Sciences, Hatfield, PA). Liver samples were fixed for 16-18 hours and ovarian tissue for up to 24 h at 4°C. Samples were transferred to 70% Ethanol until processed, dehydrated using an automated tissue processor (Leica Biosystems, Buffalo Grove, IL), embedded in paraffin, and sections were cut at 5 μm thickness for all histological applications.

PSR staining

For PSR staining, tissue sections were deparaffinized in Citrisolv (Fisher Scientific, Pittsburgh, PA) and then rehydrated in a series of graded ethanol baths (100%, 70% and 30%). Slides were then immersed in a PSR staining solution prepared by dissolving Sirius Red F3BA (Direct Red 80, C.I. 357.82, Sigma-Aldrich, St. Louis, MO) in a saturated aqueous solution of picric acid (Sigma-Aldrich, St. Louis, MO) at 0.1% w/v. Slides were incubated in the PSR staining solution for 40 minutes at room temperature. The slides were then either incubated in 0.5% glacial acetic acid (Avantor Performance Materials Inc, Center valley, PA) for a total of four, 7-minute washes or incubated in 0.05 M hydrochloric acid (Fisher Scientific) for 90 seconds. Excess acidified water was carefully wicked away from the tissue sections, and the tissue was rapidly dehydrated in 100% ethanol (a total of three, 30-second incubations). The slides were cleared in Citrisolv for five minutes and mounted with Cytoseal XYL (Fisher Scientific). For each independent experiment, all slides used for PSR staining were processed at the same time to minimize variation in staining intensity.

PSR imaging

Brightfield images were taken with an EVOS FL Auto Cell Imaging system (Thermo Fisher, Waltham, MA) using a 20X or 40X objective. To view entire ovary sections, scans comprised of a series of individual images were taken across the tissue and then automatically stitched together using the EVOS software. To quantify the area of ovarian tissue that was positive for PSR staining we followed the protocol as described: http://rsbweb.nih.gov/ij/docs/examples/stained-sections/index.html (access date February 2016). In brief, for each animal, two non-overlapping images were taken of each section at 20X magnification using the EVOS FL Auto. ImageJ was used to quantify the area of positive PSR staining above a threshold that was set based on the staining in the oldest animal for

each mouse strain. This threshold was kept constant for all images analyzed for each particular mouse strain. Sections from a total of N = 3 young and N = 3 old CB6F1 mice and a total of N = 22 CD1 mice across an aging continuum were analyzed.

For epifluorescence imaging, we used the EVOS FL Auto Cell Imaging system equipped with the following LED light cubes: Texas Red (Ex 585/29 nm; Em 624/40 nm), Green Fluorescent Protein (GFP) (Ex 470/22 nm; Em 510/42 nm), and DAPI (Ex 357/44 nm; Em 447/60 nm). To detect collagen, the Texas Red light cube was used and the light settings and exposure times were set for the samples with the most intense PSR staining (21 and 22 month old CD1 ovaries and 14-17 month old CB6F1 ovaries). These settings were then kept constant when imaging all other ovary sections. The appropriate GFP and DAPI light cube imaging settings were established using an ovarian tissue section that had been processed for immunocytochemistry with known green and blue fluorescence (Supplemental Figure 1B). In brief, immunofluorescence with a primary antibody against the oocyte specific protein, MSY2 (generous gift from R. Schultz. University of Pennsylvania), was performed and detected using a Fluorescein TSA detection kit (Perkin Elmer, Waltham, MA). Nuclei were visualized with Vectashield containing DAPI (4',6-diamidino-2-phenylindole) (Vector Laboratories, Burlingame, CA). The settings optimized with this sample were then kept constant when imaging the PSR stained ovarian sections. All post-processing adjustments of brightness were done equivalently across images using ImageJ software (Schneider, et al. 2012).

PSR stained tissue sections were also imaged using a Leica SPE confocal configured with a Leica DM550 Q upright microscope with an ACS APO 63X/1.30 Oil CS objective (Leica Microsystems Inc, Buffalo Grove, IL). The 532 nm solid state laser was used for excitation and 0.4 μm optical sections were taken through each sample.

To analyze the birefringence of ovarian tissue stained with Picrosirius Red, we used circularly polarized light microscopy on an Abrio system on an inverted Nikon Eclipse TE-300 equipped with 20X and 40X objectives (Pol-scope; Cambridge Research & Instrumentation, Inc., Oosight Imaging System, Woburn, MA). The Abrio software was used to determine the orientation of the samples' birefringence properties.

Hydroxyproline assay

To quantify the collagen content in ovarian tissue, a hydroxyproline assay was performed as previously described (Reddy and Enwemeka 1996). In brief, ovaries were hydrolyzed in 100 μL of water and 100 μL of 12.1 N hydrochloric acid and incubated at 120°C in a dry bath incubator for 3h. Samples were vortexed every 30 minutes during this incubation period. Samples were then centrifuged for 10 minutes at 10,000 × g. Five and 10 microliters of the supernatant from the hydrolyzed tissues were transferred to a 96-well plate to which 100 μL of Chloramine T reagent (Reddy and Enwemeka 1996) was added and allowed to incubate at room temperature for 25 minutes. Then, 100 μL of Ehrlich's Solution [1M 4-(dimethylamino)benzaldehyde in 1-propanol/60% perchloric acid (3:1, v/v)] was added to each well and incubated at 60°C for 35 minutes in a non-humidified, laboratory oven. After this incubation, the absorbance of all samples at 550 nm was measured in a microplate reader. A standard curve of known hydroxyproline concentrations was created from which

the concentration of hydroxyproline was calculated for each sample. Collagen contains roughly 12.5% hydroxylated prolines; therefore to extrapolate the amount of collagen that is present in ovarian tissue per mg of tissue we divided the value for the hydroxyproline concentration by 12.5%. For each assay, a total of 4 ovaries was pooled and hydrolyzed for each age group (reproductively young and old CB6F1 females). The assay was repeated four times, with technical replicates included for each. The fold change was calculated by normalizing to the average collagen values from the reproductively young ovaries for each trial. Fibrotic liver from chronically CCl_4-exposed mice served as positive controls while liver from vehicle treated mice served as negative controls for the assays.

Additional histological staining

For hematoxylin and eosin (H&E) staining, tissue sections were stained following a standard H&E staining protocol, cleared with Citrisolv (three - 5 minute incubations), and mounted with Cytoseal XYL. For Periodic Acid Schiff (PAS) staining, slides were deparaffinized in Citrisolv, rehydrated in graded ethanol baths (100%, 95%, 80% and 70%), and washed in RO water. Slides were then immersed in 0.5% periodic acid (Fisher Scientific) for 5 minutes, washed (four - 5 minute incubations) in RO water, immersed in Schiff's Reagent (Fisher Scientific) for 15 minutes, rinsed in running RO water for 10 minutes, and counterstained with hematoxylin. Slides were then dehydrated in graded ethanol baths, cleared in Citrisolv, and mounted with Cytoseal XYL.

For autofluorescence detection, tissue sections were deparaffinized, rehydrated in graded ethanol baths, and washed in RO water. Slides were then incubated in Tris-buffered saline supplemented with 0.1% Tween-20 (TBS-T, three - 10 minute incubations, and mounted with Vectashield with or without DAPI. All imaging was performed using the EVOS FL Auto Cell Imaging system.

Immunofluorescence and immunohistochemistry

For detecting macrophages in ovarian tissue sections, immunofluorescence was performed. In brief, tissues sections were deparaffinized in Citrisolv and rehydrated in a series of graded ethanol baths (100%, 95%, 85%, 70% and 50%). Antigen retrieval was performed using 10x Reveal Decloaker (Biocare Medical, Concord, CA) according to the manufacturer's instructions. Slides were rinsed in TBS-T, incubated in 30% hydrogen peroxide (Fisher Scientific) followed by incubations in avidin and biotin blocking solutions for 15 minutes at room temperature (Vector Laboratories, Burlingame, CA). The tissue sections were then incubated in blocking solution [10% normal goat serum (Vector Laboratories) and 0.4% Triton X-100 (Fisher Scientific) diluted in TBS] for 1 hour at room temperature and then incubated overnight at 4°C in primary antibody at 1:50 dilution (rat anti-mouse F4/80, Bio-Rad, Hercules, CA). Slides were rinsed in TBS-T and incubated in 1:100 dilution of secondary antibody (biotinylated anti-rat IgG, Vector Laboratories) for two hours at room temperature. The slides were rinsed and incubated in ABC reagent (Vector Laboratories) for 30 minutes at room temperature. Signal amplification was performed using the Fluorescein TSA kit according to the manufacturer's instructions (Perkin Elmer). The slides were mounted with Vectashield containing DAPI. We used the EVOS FL Auto Imaging automated cell counting software with watershed algorithm to determine the number of

F4/80 positive cells (fluorescein-positive) cells and total number of cells (DAPI-positive) in ovarian sections. Intensity thresholds were set according to secondary only controls. To determine the percentage of F4/80 positive cells, we reported the average number of fluorescein-positive cells over the total number of cells for each image. A minimum of five images was analyzed for each ovary (N = 3 reproductively young and N = 3 reproductively old CB6F1 females).

For detection of alpha-smooth muscle actin (α-SMA), ovarian tissue sections were deparaffinized and antigen retrieval was performed as above. Primary and secondary antibody incubations were performed using Vector Mouse on Mouse (M.O.M) kit (Vector Laboratories) and Vector ABC kit (Vector Laboratories) according to the manufacturer's protocols. Detection was done via 3’3’-Diaminobenzidine (DAB) staining using the DAB Peroxidase (HRP) Substrate Kit (Vector Laboratories). The primary antibody used was anti-alpha smooth muscle actin (ab7817) at 1:250 dilution (Abcam, Cambridge, United Kingdom). All imaging was performed using the EVOS FL Auto Cell Imaging system.

Electron Microscopy

Ovaries were bisected longitudinally using a scalpel and fixed in 2% glutaraldehyde in 0.1M sodium cacodylate buffer. The tissue was transferred to 5 ml screw cap glass vials for processing. The tissue was rinsed in fresh cacodylate buffer for 20 min and then post fixed in 1% buffered osmium tetroxide for 1 hour. The samples were rinsed in 3 exchanges of deionized distilled water and then dehydrated through a graded series of ethanols (50%, 70%, 80%, 95%, 100%). Each step was done for 20 min and repeated twice. The tissue was placed in propylene oxide for 20 min and then into a mixture of half volume propylene oxide and half volume Embed 812 medium mixture (Electron Microscopy Sciences Inc), overnight. The half and half mixture was removed the next day and 100% Embed mixture was added to the sample and allowed to stand for 1 hour. Resin was removed and replaced with fresh Embed mixture and placed in a 65°C oven to polymerize overnight. Samples were sectioned using a Diatome diamond knife on a Leica UC-7 ultra microtome. Sections were cut at 1 micron until areas of interest were noted and then sections were cut at 70 nm and picked up on 300 mesh thin bar grids (EMS, Inc.) Section contrast was achieved through exposure to 3% uranyl acetate and Sato's Lead stain and viewed with a JEM 1400 TEM (J.E.O.L. Inc) at 100kv.

Gene expression analysis

One ovary from each mouse was placed in RNA later solution (Ambion, Grand Island, NY) to stabilize RNA (N = 4 reproductively young and N = 4 reproductively old CB6F1 females). A bead homogenizer (FastPrep 24, MP Biomedical, Solon, OH) was used to homogenize tissue in RLT buffer (RNeasy Mini Kit, Qiagen, Valencia, CA) containing β-mercaptoethanol. The RNeasy Mini kit was used to isolate RNA, and 0.85 μg of RNA was reverse transcribed to cDNA using a Retroscript kit (Life Technologies/Ambion). A BioRad CFX384 (Hercules, CA) machine was used for real time polymerase chain reaction (PCR). 18S was used as the housekeeping gene, and gene expression was calculated using the $2^{-\Delta\Delta Ct}$ method. Results are expressed as fold change in expression over young mice. Primers came from Primer Bank (Spandidos, et al. 2008, Spandidos, et al. 2010, Wang and Seed

2003) unless otherwise stated and include *Il1β* F: GAAATGCCACCTTTTGACAGTG R: CTGGATGCTCTCATCAGGACA (Primer Bank ID: 118130747b1), *Il6* F: CTGCAAGAGACTTCCATCCAG R: AGTGGTATAGACAGGTCTGTTGG (Primer Bank ID: 13624310b1), *Il10* F: GCT CTT ACT GAC TGG CAT GAG R: CGC AGC TCT AGG AGC ATG TG (Primer Bank ID: 6754318A1), *Ccl2* F: AGGTCCCTGTCATGCTTCTG R: TCTGGACCCATTCCTTCTTG (Pascual, et al. 2011), *Tnfα* F: CCCTCACACTCAGATCATCTTCT R: GCTACGACGTGGGCTACAG (Pritchard, et al. 2010), *Ccl5* F: TTTGCCTACCTCTCCCTCG R: CGACTGCAAGATTGGAGCACT (Primer Bank ID: 164698427b1). All primer oligonucleotides were synthesized by Integrated DNA Technologies (Coralville, IA) and used at 0.1 μM in real time PCR reactions.

Cytokine antibody arrays

Ovaries from reproductively young and old CB6F1 mice were harvested, pooled according to age cohort (N = 4 mice per age group) and cultured on 0.4 μm, 30 mm Millicell inserts (Merck Millipore Inc, Billerica, MA) in 6-well dishes for a total of 2.5 hours in a humidified atmosphere of 5% CO_2 in air at 37°C. Each well contained 1.5 ml of culture media, and ovaries were overlaid with a thin film of media. The culture media was αMEM GlutaMAX (Thermo Fisher) supplemented with 0.1% bovine serum albumin (Thermo Fisher), 1× ITS-X (Thermo Fisher), 0.05 mg/ml L-ascorbic acid (Sigma-Aldrich), and 1× PenStrep (Thermo Fisher). Media alone was included as a control. Following culture, 0.5 ml of the spent culture media from each group was combined with 0.5 ml blocking buffer supplied with the cytokine antibody array kit and then run on the RayBio C-Series Mouse Cytokine Antibody Array C1 according to the manufacturer's protocol (RayBiotech, Norcorss, GA). Data analysis was done according to the manufacturer's instruction. In brief, raw numerical densitometry data was extracted from the arrays by measuring the mean integrated density of a defined area for each spot using ImageJ. Background subtraction was performed using the blank values, and positive control normalization was done using the media only array as a reference. Signals from the media only array were subtracted, and the fold change between young and old samples was calculated. This experiment was repeated twice.

Statistical analysis

Statistical analyses were performed using Microsoft Excel or Graphpad-Prism Software Version 6.0f (La Jolla, CA). For gene expression analysis, a two-tailed t-test for significance and a Q-test was used to remove any outliers. For other assays, changes between groups were analyzed by Pearson's Correlation or a t-test, and a P-value < 0.05 was considered significant.

Results

Picrosirius Red (PSR) staining reveals collagen networks in the ovary by brightfield microscopy

Upon binding to collagen fibers, PSR results in a dark red stain that is readily visualized by brightfield microscopy whereas cytoplasmic regions appear yellow or faint pink (Junqueira, et al. 1979, Junqueira, et al. 1978). We first validated our staining conditions using liver

samples from mice treated with a chronic CCl_4 regimen that is known to induce fibrosis in distinct regions of the liver (Constandinou, et al. 2005, Pritchard and Nagy 2010, Weber, et al. 2003). In this model, fibrotic septae connect the central veins throughout the liver in a typical 'chicken-wire' pattern characteristic of bridging fibrosis. In control mice, the majority of the liver tissue appeared yellow or light pink, and there was minimal, but expected, PSR staining around the hepatic vessels (Figure 1A, arrows and asterisks). However, in the CCl_4-treated liver samples, there was significant PSR-positive staining surrounding and extending from the central veins (Figure 1B, asterisks). These results confirmed that we could use PSR-staining to distinguish between fibrotic and non-fibrotic tissue.

We next examined PSR staining in ovarian tissue (Figure 1C). For these characterization studies, we used ovarian tissue from reproductively old mice (21-22 months old), as fibrosis increases with age in several tissues (Horn and Trafford 2015, Kapetanaki, et al. 2013, Sangaralingham, et al. 2016). We found a prominent network of intense PSR-stained collagen fibers throughout the ovarian stroma (Figure 1C). In general, the bulk of the non-fibrotic regions in the ovary stained a darker pink compared to the liver, irrespective of fixation conditions (Figure 1 and data not shown). Background pink staining may be due to structures that contain basic proteins, suggesting differing tissue compositions between the liver and ovary (Nielsen, et al. 1998). This background is largely eliminated when visualizing PSR by other methods as described below.

PSR staining exhibits red fluorescence and birefringence which enhances visualization of collagen fibers in the ovary

In cardiac tissue, PSR-stained collagen fibers produce strong fluorescence in the red wavelength (Dolber and Spach 1993, Vogel, et al. 2015). To examine the fluorescent properties of PSR staining in ovarian tissue, we visualized sections by epifluorescence microscopy. We found that the collagen fibers that stained intense red with PSR by brightfield microscopy corresponded to regions of intense fluorescence when examined with a Texas Red light cube (Figures 2A-B, Supplemental Figure 1). This fluorescence was specific to the PSR-stained fibers as no signal was observed when adjacent unstained sections were examined (Figures 2C-D and Supplemental Figure 1). Furthermore, PSR-stained tissue only exhibited fluorescence in the near red wavelength as no appreciable signal was detected when the samples were visualized with either GFP (green wavelength) or DAPI (blue wavelength) light cubes (Supplemental Figure 1). The red fluorescence signal eliminated the background pink cytoplasmic staining that was prominent in the ovary by brightfield microscopy, further confirming the specificity of PSR for collagen fibers (Figure 1C, Figures 2A-B, Supplemental Figure 1).

To obtain a more detailed view of the arrangement of the PSR-stained structures within the ovary, we examined histological sections by confocal microscopy. We found that PSR staining detected fibers that ranged ~ 5-15 μm in diameter throughout the ovary that were composed of linearly arranged bundles of individual fibrils (Figures 2E-F). This fluorescence was only observed with the 532 nm laser (Figures 2E-F and data not shown). These results are consistent with collagen fibers, which are reported to be 1-20 μm wide, and

therefore provide further validation of the specificity of the PSR staining within the ovary (Ushiki 2002).

To further confirm that PSR detects collagen fibers in the ovary, we imaged PSR-stained ovarian sections using circularly polarized light microscopy. This technique can be used to determine a specimen's optical anisotropy, which is a consequence of its molecular order and architecture (Mehta, et al. 2013). Biological structures, such as collagen, are composed of filaments that are anisotropic themselves and can exhibit birefringence or anisotropy of refraction (Mehta, et al. 2013). PSR staining enhances the natural birefringence of collagen when examined under polarized light because the PSR dye molecule (F3BA) binds to the tertiary groove of collagen I and III fibrils alongside the fiber axis (Lattouf, et al. 2014, Street, et al. 2014). Additionally, birefringence is amplified because approximately 120 dye molecules bind per collagen molecule. The signal obtained from PSR staining, especially when combined with enhanced birefringence, is therefore considered highly specific for collagen (Junqueira, et al. 1979, Lattouf, et al. 2014, Street, et al. 2014, Whittaker, et al. 1994). When imaged in this manner, collagen bundles appear bright relative to a black background. Using an Abrio Liquid Crystal (LC) PolScope, we detected the birefringent properties of PSR-stained ovarian tissue sections and found that the highly birefringent regions corresponded to the most intense red staining visualized by brightfield microscopy (Figures 3A-B), which is consistent with our observations with red fluorescence (Figure 2B). Moreover, we used the LC-PolScope software to determine the orientation of the molecular order or birefringence in the PSR-stained ovarian tissue. As is evident by the pseudocolor polarized light image superimposed with retardance vectors, the birefringent PSR-stained collagen bundles are regularly ordered (green retardance vectors facing the same direction) and are arranged with multiple orientations (different colors) in the ovary (Figure 3C). Taken together, these multiple imaging approaches (brightfield, epifluorescence, confocal, and polarized light) provide strong evidence that PSR staining detects highly ordered collagen fibers in the mouse ovary.

PSR staining demonstrates an age-associated increase in fibrosis in the mouse ovary

Following the validation of PSR staining as an indicator of fibrous collagen in the ovary, we then used this histological tool to evaluate whether fibrosis increased in the mouse ovary with advanced reproductive age. The mouse is an important model for reproductive aging, since several mouse strains exhibit reproductive aging phenotypes that parallel what occurs in human, including loss of the ovarian reserve, altered endocrine function, increased egg aneuploidy, and subfertility (Chiang, et al. 2010, Hirshfeld-Cytron, et al. 2011, Hornick, et al. 2015, Merriman, et al. 2012, Treff, et al. 2016). We performed PSR staining on an aging series of ovarian tissue sections from mice of the CD1 strain that ranged in age from 6 weeks to 22 months (Figure 4). In ovaries from animals of all ages, some PSR staining was observed as expected because structures such as follicles, the ovarian surface epithelium, and blood vessels contain collagen (Berkholtz, et al. 2006) (Figure 4). However, fibrotic foci characterized by intense PSR staining visualized using both brightfield and fluorescence microscopy, were visible in the ovarian stroma beginning between 7 and 9 months of age (Figures 4C-D, 4C’-D’, and 4C”-D”). These foci appeared to expand such that fibrosis was prominent throughout the ovarian stroma of animals between 18-22 months of age (Figures

4E-F, 4E'-F', and 4E"-F"). In fact, there was a significant positive linear correlation between animal age and the amount of PSR-positive staining observed per ovarian section (Figures 5A-D; P = 0.0006).

The reproductive age-associated expansion of PSR staining and fibrosis was not unique to this specific mouse strain as we observed a similar phenomenon within the ovarian stroma of CB6F1 mice as well (Figures 5E-G and Figures 6A-D). Specifically, ovaries from the reproductively old cohort of CB6F1 mice had nearly double the amount of PSR-positive staining in the ovarian stroma relative to the reproductively young cohort (Figures 5E-G; 6-12 weeks old vs. 14-17 months old; P = 0.03). To further quantify this age-associated fibrosis, we compared total collagen levels in ovaries from reproductively young and old CB6F1 mice using a hydroxyproline assay (Figure 6E-H). Hydroxylated proline is a post-translational modification found almost exclusively in connective tissue collagen, and thereby hydroxyproline levels can be used as a surrogate measure of collagen metabolism and regulation (McAnulty 2005, Reddy and Enwemeka 1996). Proline hydroxylation allows the sharp twisting of the collagen helix and stabilizes the collagen structure. Notably, elevated hydroxyproline levels reflect higher collagen levels and are observed in fibrotic pathologies (McAnulty 2005). We first validated the hydroxyproline assay using liver tissue from CCl_4-treated and control mice, and as expected, we observed a higher collagen content in the CCl_4-treated mice with known fibrosis (2-fold increase, data not shown). We then used this assay to extrapolate and compare the amount of collagen per mg of ovarian tissue from reproductively young and old mice. In each trial performed, we consistently observed a higher level of total collagen in ovaries from reproductively old mice compared to reproductively young mice, and this reproductive age-associated increase was significant in three of the four trials (Figures 6E-H). When analyzed together, these trials represent an average 1.6-fold age-associated increase (P = 0.004). This increase in ovarian hydroxyproline content mirrors the results obtained with PSR staining and further confirms that the aging ovary includes a fibrotic microenvironment (Figures 4-6).

Ovarian fibrosis is associated with multinucleated macrophage giant cells

Fibrosis is associated with inflammation, so we next investigated whether there were reproductive age-associated changes in immune cells within the ovary (Libby 2007, Sziksz, et al. 2015). Specifically we examined macrophages in ovarian sections from CB6F1 mice using an antibody against F4/80, a cell-surface membrane protein that is expressed at high levels in various mouse macrophages (Murray and Wynn 2011). We found that there were similar numbers of F4/80-positive cells in ovaries of reproductively young and old mice, comprising 23.9% ± 1.7% and 25.4% ± 0.83% of the total cell number, respectively (Figure 7, inset, P = 0.45). This observation is consistent with the well-documented role of macrophages in numerous ovarian processes including folliculogenesis, ovulation, and corpus luteum formation and regression (Wu, et al. 2004). These macrophages had varying morphologies, including small spindle-shaped macrophages and ovoid macrophages, suggesting sub-populations with differing functions (Asano 2012) (Figures 7B, D).

Although we did not observe any obvious age-associated difference in the percentage of F4/80-positive cells in the ovarian stroma, we did document a unique cell population that

was consistently observed in tissue from reproductively old CB6F1 mice relative to young mice (Figure 8; Table I). Specifically, these cells stained a light brown with H&E and were enlarged, foamy, and often multinucleated (Figures 8C-F and Figure 9A, insets). By electron microscopy, these cells had vacuoles and inclusion bodies of various sizes indicative of phagocytosis of non-digestible material (Figure 8E). Moreover, these cells exhibited high levels of autofluorescence relative to the surrounding tissue, which may be due to aggregated polymers resulting from oxidation of proteins and lipids (Figure 8F, inset) (Porta 2002). Cells with the same characteristics were also observed in the CD1 mouse strain and were associated with advanced reproductive age (Table I and data not shown). These cells were absent in mice ≤ 7 months of age, present in 70% of mice between 10-14 months of age, and present in 100% of mice ≥ 18 months of age (Table I). Thus, these multinucleated giant cells correlate with increased age-associated fibrosis in the ovarian stroma.

The multinucleated giant cells were identified as macrophages because they stained positive for the F4/80 marker (Figures 9B, D). The F4/80 staining at the cell periphery, however, was variable. In some enlarged macrophages that were still individualized, the staining was at the periphery (Figure 9B, arrow), but in other cells within the cluster, F4/80 expression was reduced and absent from the cell surface (Figures 9B, D). Due to their phagocytic function, multinucleated macrophage giant cells are enriched in polysaccharides that are distributed throughout the cytoplasm in small granules or in compact masses that stain positive with Periodic Acid Schiff (PAS) (Sobolev 1959). Using this histological stain, we demonstrated that the regions of the ovarian stroma that contain these multinucleated macrophage giant cells also stain intensely with PAS (Figures 9B, D, insets). Taken together, these results suggest that macrophage fusion into multinucleated giant cells is a hallmark of the ovarian stroma during reproductive aging. Interestingly, these multinucleated giant cell macrophages were often observed in close proximity with cells that stained positive for α-smooth muscle actin (α-SMA) (Figure 9C). α-SMA is a marker characteristic of fibroblast activation, which is associated with enhanced collagen secretion and, therefore, represents a critical transition in fibrogenesis (Hinz 2016). In lung and liver, pro-fibrotic macrophages produce factors that regulate the proliferation, survival, and activation status of cells with fibrogenic potential (Murray and Wynn 2011).

Ovarian fibrosis is associated with an inflammatory microenvironment

To verify whether reproductive age-related ovarian fibrosis is associated with increased inflammation, we interrogated the gene expression profiles of several genes involved in fibrosis and inflammation in whole ovaries isolated from reproductively young and old CB6F1 mice (Figure 10). Specifically, we examined the expression of major pro-inflammatory cytokines that are also known to have pro-fibrotic functions, including *Il1b*, *Il6*, and *Tnfa* (Sziksz, et al. 2015, Wick, et al. 2013, Wynn and Barron 2010) (Figures 10A-C). These genes all showed higher levels of expression in ovaries from reproductively old mice relative to young mice, with *Il1b* and *Tnfa* expression being significantly different between the age cohorts. In addition, we examined the expression pattern of genes involved in immune cell recruitment. *Ccl2* encodes monocyte chemoattractant protein 1, which recruits monocytes to sites of inflammation where they ultimately differentiate into macrophages, and *Ccl5* is involved in general leukocyte and fibroblast recruitment

(Mantovani, et al. 2004, Sahin and Wasmuth 2013). Both *Ccl2* and *Ccl5* expression were significantly increased in ovaries from reproductively old mice relative to young counterparts (Figures 10D-E). Finally, we examined the expression of *Il10,* which is typically considered an anti-inflammatory cytokine with anti-fibrotic functions (Sziksz, et al. 2015) (Figure 10F). Although *Il10* expression was higher in ovaries from reproductively old mice compared to young mice, this difference was not significant. However, IL-10 inhibits TNF-alpha production, and thus, the observed increase in IL-10 may represent a countermeasure within the ovary to modulate fibrosis (Denys, et al. 2002).

To further assess the inflammatory microenvironment of the aging ovary, we performed cytokine antibody arrays on conditioned culture media from ovaries isolated from reproductively young and old CB6F1 mice (Figures 10G-H). We only cultured the ovaries for 2.5 hours to avoid confounding results due to tissue ischemia and necrosis. Due to this short-term culture and the small amount of tissue, we only detected signals from five cytokines in the spent culture media, including IL-6, CCL2, CCL5, TNFR1, and IL12 p70 (Figure 10H). Despite the limitations of this approach, however, we identified a prominent and significant 15-fold increase in IL-6 secretion in ovaries from reproductively old mice compared to young mice (Figure 10H), which parallels the increase observed at the gene expression level (Figure 10B). The cytokine expression and secretion data, along with the presence of multinucleated macrophage giant cells, are consistent with a highly inflammatory milieu within the aging ovary.

Discussion

In this study, we used PSR, a classic and highly-specific histological dye for collagen I and III fibers, to evaluate fibrosis within ovarian tissue (Junqueira, et al. 1979, Junqueira, et al. 1978). Using various imaging approaches, we validated that PSR stains this ovarian ECM network a bright red and also exhibits strong red fluorescence and birefringence. Histopathologists commonly use PSR staining to evaluate degrees of fibrosis because this method is cost-effective, simple, and consistent relative to other immunohistochemical, molecular, and biochemical approaches to assess fibrosis (Coleman 2011). Using PSR staining, we determined that fibrosis within the ovarian stroma increased with advanced reproductive age in both CD1 and CB6F1 mouse strains, and this is consistent with the increased collagen levels that we quantified in ovaries from reproductively old animals using the biochemical hydroxyproline assay. In ovaries from the oldest animals (>20 months of age), PSR staining was the most prominent, and in some cases, accounted for > 35% of the total ovarian area. This extensive fibrosis resembles what is observed in hepatocyte nodules in liver cirrhosis or in schistosome-induced granuloma formation (Bataller, et al. 2011, Mathurin and Bataller 2015, Olveda, et al. 2014). Although ovarian fibrosis was most severe in the oldest animals, regions of fibrosis were evident within the tissue earlier. For example, we consistently documented fibrotic foci and multinucleated macrophage giant cells in the ovarian stroma in mice that were 14-17 months of age, which based on a linear extrapolation of age, would roughly correspond to women who are approximately 38-45 years of age. Importantly in both mice and humans, this period of the reproductive lifespan is already characterized by quantifiable changes in egg quality – namely a dramatic increase in the incidence of aneuploidy upwards of 60% (Jones and Lane 2013). Thus, the changes in the

ovarian microenvironment we observed are coincident with this known decrease in egg quality and may play a causative role.

Although it is evident that fibrosis increases in the ovarian stroma with advanced reproductive age, the mechanism by which this occurs is still unknown. The ovary is composed of several ECM matrices including the follicular basal lamina matrix, the cumulus-oocyte matrix, and the stromal matrix (Irving-Rodgers, et al. 2010). Through the processes of folliculogenesis and ovulation, the ovary undergoes constant cycles of connective tissue remodeling and wound healing which requires a complex interplay between matrix metalloproteinases (MMPs) and tissue inhibitors of metalloproteinases (TIMPs) (Curry and Osteen 2001). The age-associated increase in fibrosis could be due to increased synthesis and deposition of collagen or other ECM components and/or altered post-translational modifications. Consistent with this possibility, we observed α-SMA-positive cells in the ovarian stroma, which may correspond to a myofibroblast population that produces excess collagen (Hinz 2016). Alternatively, or in combination with increased ECM production, there may be an age-associated change in the homeostasis of ECM through an imbalance of the activities of MMPs and TIMPs. Distinguishing between these various mechanisms is currently under investigation.

In addition to a prominent age-associated increase in fibrosis, we also documented increased expression of genes involved in immune cell recruitment that occurred concomitantly with the presence of a unique population of multinucleated macrophage giant cells in ovaries from reproductively old mice. Macrophages undergo fusion with other macrophages to form multinucleated giant cells and are a hallmark of chronic inflammation (Helming and Gordon 2009, McNally and Anderson 2011). Multinucleated giant cells are observed in cases of pathological infection, sarcoidosis, rheumatoid arthritis, certain neoplasias, and at sites of device or biomaterial implants (McNally and Anderson 2011). Although, the biological significance of macrophage fusion and multinucleation is not well understood, it has been proposed that this process enhances the phagocytic function of the cells through increased size which allows extracellular degradation of large targets (Helming and Gordon 2009). These multinucleated giant cells are reminiscent of osteoclasts, which have a significant capacity to degrade large areas of bone and other poorly degradable material (Helming and Gordon 2009). Thus, this cell population in the aged ovary may be involved in resolving fibrotic regions of tissue. Interestingly, this population of cells in the ovary had variable F4/80 staining, with some cells exhibiting a peripheral pattern of expression while others showing decreased expression. The down-regulation of F4/80 may reflect the activation status of this cohort of macrophages as has been observed in other examples of fibrotic progression and resolution (Ramachandran, et al. 2012).

Macrophages are also major secretory cells that release cytokines, chemokines, and growth factors that greatly influence proper follicle development (Tingen, et al. 2011). Our gene expression results demonstrate that there are increased levels of pro-inflammatory cytokines within the aging ovary. IL-6 secretion from the ovary was significantly increased with advanced reproductive age. This is of particular interest because serum IL-6 levels increase in humans with age, and IL-6 may mediate fibrosis by transcriptional activation of collagen or by stimulation of cytokines that upregulate collagen in an autocrine manner (Maggio, et

al. 2006, O'Reilly, et al. 2013). Further defining the inflammatory milieu of the aging ovary and determining whether multinucleated macrophage giant cells are a cause or consequence of chronic inflammation are warranted and currently under investigation. Ultimately modulating pro-inflammatory pathways may be an important therapeutic avenue for prolonging reproductive lifespan because, for example, in a mouse knockout model of the pro-inflammatory cytokine IL-1α, the ovarian lifespan, pregnancy rate, and litter size were all increased relative to age-matched controls (Uri-Belapolsky, et al. 2014).

A similar population of enlarged macrophage cells was observed previously in the ovarian stroma of aged C57B/6J mice, thereby corroborating our findings in CB6F1 and CD1 mice (Asano 2012). These enlarged macrophages were also characterized by a frothy cytoplasm with polymorphic inclusion bodies and lysosomes, multiple nuclei, and intense autofluorescence (Asano 2012). It was also noted that there was a reproductive age-associated accumulation of non-heme iron in the ovarian stroma and that the subpopulation of enlarged macrophages had particularly high levels of nonheme ferric iron (NHF[III]), non-heme ferrous iron (NHF[II]), and oxidative stress (Asano 2012). This non-heme iron accumulation in the ovary with age may result from heme oxygenase-1-mediated heme degradation during follicular atresia and luteal regression (Asano 2012). Disruption of iron homeostasis in several organs, including the liver, heart, and pancreas, leads to organ fibrosis (Ramm and Ruddell 2010). Thus, it is tempting to speculate that iron accumulation in the aging ovary may be a mechanism driving fibrosis. In addition, whether these changes are regulated hormonally is also of great interest as aromatase knockout mice have ovaries with significant follicle loss, a large influx of macrophages, and an increase in collagen deposition (Britt, et al. 2000).

Taken together, we used a combination of imaging approaches to establish PSR staining as an important tool for studying fibrosis in the ovary and documented a prominent reproductive age-associated increase in fibrosis within the ovarian stroma that was coincident with a population of multinucleated macrophage giant cells and increased inflammation. Investigating how the extra-follicular ovarian microenvironment changes with age will improve our understanding of ovarian biology but also has broader implications for women's health. For example, ovarian fibrosis is a key feature of Polycystic Ovarian Syndrome (PCOS), which is also accompanied by chronic low-grade inflammation (Bulut, et al. 2015). Additionally, ovarian fibrosis is an unintended consequence of iatrogenic insults such as chemotherapy and radiation (Stroud, et al. 2009). Quantifying ovarian fibrosis using methods, such as multi-modal magnetic resonance elastography, could therefore serve as a non-invasive metric of ovarian function (Wood, et al. 2015). Furthermore, therapeutic strategies that target fibrotic remodeling may have a promising future in improving reproductive function in the context of age-related infertility, PCOS, and fertility preservation.

Supplementary Material

Refer to Web version on PubMed Central for supplementary material.

Acknowledgements

We acknowledge John Kelsh for his initial observations which inspired this study, Dr. Aaron Varghese for contributing to literature searches and providing technical assistance, Dr. Teresa K. Woodruff for allowing us to use the LC-Polscope in her laboratory, and Dr. Dale Abrahamson for useful discussions.

Funding

This work was supported by the Center for Reproductive Health After Disease (P50 HD076188 to F.E.D.) from the National Centers for Translational Research in Reproduction and Infertility (NCTRI), the Centers of Biomedical Research Excellence (P20 GM104936 to F.E.D.), the National Institutes of Health, National Center for Research Resources (P20 RR021940 to M.T.P.), the National Institute of General Medical Sciences (P20 GM103549 to M.T.P.), and the National Institute of Environmental Health Sciences "Training Program in Environmental Toxicology" (T32 ES007079 to J.M.M.]). In addition, summer student research for this project was supported by the Kansas Institutional Development Award (IDeA) (P20 GM103418). The Electron Microscopy Research Laboratory and Anatomy/COBRE Confocal Imaging Facility at KUMC are supported in part by NIH COBRE 9P20GM104936. The JEOL JEM-1400 TEM used in the study was purchased with funds from S10RR027564. The Histology Core at KUMC is supported by NICHD P30 HD002528 (Kansas IDDRC).

References

Alves A, Gritsch K, Sirieix C, Drevon-Gaillot E, Bayon Y, Clermont G, Boutrand JP, Grosgogeat B. Computerized histomorphometric study of the splenic collagen polymorphism: A control-tissue for polarization microscopy. Microsc Res Tech. 2015; 78:900–907. [PubMed: 26238067]

Asano Y. Age-related accumulation of non-heme ferric and ferrous iron in mouse ovarian stroma visualized by sensitive non-heme iron histochemistry. J Histochem Cytochem. 2012; 60:229–242. [PubMed: 22108647]

Bataller R, Rombouts K, Altamirano J, Marra F. Fibrosis in alcoholic and nonalcoholic steatohepatitis. Best Pract Res Clin Gastroenterol. 2011; 25:231–244. [PubMed: 21497741]

Berkholtz CB, Lai BE, Woodruff TK, Shea LD. Distribution of extracellular matrix proteins type I collagen, type IV collagen, fibronectin, and laminin in mouse folliculogenesis. Histochem Cell Biol. 2006; 126:583–592. [PubMed: 16758163]

Britt KL, Drummond AE, Cox VA, Dyson M, Wreford NG, Jones ME, Simpson ER, Findlay JK. An age-related ovarian phenotype in mice with targeted disruption of the Cyp 19 (aromatase) gene. Endocrinology. 2000; 141:2614–2623. [PubMed: 10875266]

Broekmans FJ, Soules MR, Fauser BC. Ovarian aging: mechanisms and clinical consequences. Endocr Rev. 2009; 30:465–493. [PubMed: 19589949]

Bulut G, Kurdoglu Z, Donmez YB, Kurdoglu M, Erten R. Effects of jnk inhibitor on inflammation and fibrosis in the ovary tissue of a rat model of polycystic ovary syndrome. Int J Clin Exp Pathol. 2015; 8:8774–8785. [PubMed: 26464620]

Check JH, Jamison T, Check D, Choe JK, Brasile D, Cohen R. Live delivery and implantation rates of donor oocyte recipients in their late forties are similar to younger recipients. J Reprod Med. 2011; 56:149–152. [PubMed: 21542533]

Chiang T, Duncan FE, Schindler K, Schultz RM, Lampson MA. Evidence that weakened centromere cohesion is a leading cause of age-related aneuploidy in oocytes. Curr Biol. 2010; 20:1522–1528. [PubMed: 20817534]

Coleman R. Picrosirius red staining revisited. Acta Histochem. 2011; 113:231–233. [PubMed: 20188402]

Constandinou C, Henderson N, Iredale JP. Modeling liver fibrosis in rodents. Methods Mol Med. 2005; 117:237–250. [PubMed: 16118456]

Curry TE Jr. Osteen KG. Cyclic changes in the matrix metalloproteinase system in the ovary and uterus. Biol Reprod. 2001; 64:1285–1296. [PubMed: 11319131]

Denic A, Glassock RJ, Rule AD. Structural and Functional Changes With the Aging Kidney. Adv Chronic Kidney Dis. 2016; 23:19–28. [PubMed: 26709059]

Denys A, Udalova IA, Smith C, Williams LM, Ciesielski CJ, Campbell J, Andrews C, Kwaitkowski D, Foxwell BM. Evidence for a dual mechanism for IL-10 suppression of TNF-alpha production that

does not involve inhibition of p38 mitogen-activated protein kinase or NF-kappa B in primary human macrophages. J Immunol. 2002; 168:4837–4845. [PubMed: 11994432]

Dolber PC, Spach MS. Conventional and confocal fluorescence microscopy of collagen fibers in the heart. J Histochem Cytochem. 1993; 41:465–469. [PubMed: 7679127]

Heffner LJ. Advanced maternal age--how old is too old? N Engl J Med. 2004; 351:1927–1929. [PubMed: 15525717]

Helming L, Gordon S. Molecular mediators of macrophage fusion. Trends Cell Biol. 2009; 19:514–522. [PubMed: 19733078]

Hinz B. Myofibroblasts. Exp Eye Res. 2016; 142:56–70. [PubMed: 26192991]

Hirshfeld-Cytron JE, Duncan FE, Xu M, Jozefik JK, Shea LD, Woodruff TK. Animal age, weight and estrus cycle stage impact the quality of in vitro grown follicles. Hum Reprod. 2011; 26:2473–2485. [PubMed: 21669966]

Horn MA, Trafford AW. Aging and the cardiac collagen matrix: Novel mediators of fibrotic remodelling. J Mol Cell Cardiol. 2015

Hornick JE, Duncan FE, Sun M, Kawamura R, Marko JF, Woodruff TK. Age-associated alterations in the micromechanical properties of chromosomes in the mammalian egg. J Assist Reprod Genet. 2015; 32:765–769. [PubMed: 25758987]

Irving-Rodgers HF, Hummitzsch K, Murdiyarso LS, Bonner WM, Sado Y, Ninomiya Y, Couchman JR, Sorokin LM, Rodgers RJ. Dynamics of extracellular matrix in ovarian follicles and corpora lutea of mice. Cell Tissue Res. 2010; 339:613–624. [PubMed: 20033213]

Johnson JA, Tough S, O Society of, and C Gynaecologists of. Delayed child-bearing. J Obstet Gynaecol Can. 2012; 34:80–93. [PubMed: 22260768]

Jones KT, Lane SI. Molecular causes of aneuploidy in mammalian eggs. Development. 2013; 140:3719–3730. [PubMed: 23981655]

Junqueira LC, Bignolas G, Brentani RR. Picrosirius staining plus polarization microscopy, a specific method for collagen detection in tissue sections. Histochem J. 1979; 11:447–455. [PubMed: 91593]

Junqueira LC, Cossermelli W, Brentani R. Differential staining of collagens type I, II and III by Sirius Red and polarization microscopy. Arch Histol Jpn. 1978; 41:267–274. [PubMed: 82432]

Kapetanaki MG, Mora AL, Rojas M. Influence of age on wound healing and fibrosis. J Pathol. 2013; 229:310–322. [PubMed: 23124998]

Lattouf R, Younes R, Lutomski D, Naaman N, Godeau G, Senni K, Changotade S. Picrosirius red staining: a useful tool to appraise collagen networks in normal and pathological tissues. J Histochem Cytochem. 2014; 62:751–758. [PubMed: 25023614]

Libby P. Inflammatory mechanisms: the molecular basis of inflammation and disease. Nutr Rev. 2007; 65:S140–146. [PubMed: 18240538]

Maggio M, Guralnik JM, Longo DL, Ferrucci L. Interleukin-6 in aging and chronic disease: a magnificent pathway. J Gerontol A Biol Sci Med Sci. 2006; 61:575–584. [PubMed: 16799139]

Mantovani A, Sica A, Sozzani S, Allavena P, Vecchi A, Locati M. The chemokine system in diverse forms of macrophage activation and polarization. Trends Immunol. 2004; 25:677–686. [PubMed: 15530839]

Mathurin P, Bataller R. Trends in the management and burden of alcoholic liver disease. J Hepatol. 2015; 62:S38–46. [PubMed: 25920088]

McAnulty RJ. Methods for measuring hydroxyproline and estimating in vivo rates of collagen synthesis and degradation. Methods Mol Med. 2005; 117:189–207. [PubMed: 16118453]

McNally AK, Anderson JM. Macrophage fusion and multinucleated giant cells of inflammation. Adv Exp Med Biol. 2011; 713:97–111. [PubMed: 21432016]

Mehta SB, Shribak M, Oldenbourg R. Polarized light imaging of birefringence and diattenuation at high resolution and high sensitivity. J Opt. 2013; 15

Merriman JA, Jennings PC, McLaughlin EA, Jones KT. Effect of aging on superovulation efficiency, aneuploidy rates, and sister chromatid cohesion in mice aged up to 15 months. Biol Reprod. 2012; 86:49. [PubMed: 22053097]

Montes GS, Junqueira LC. The use of the Picrosirius-polarization method for the study of the biopathology of collagen. Mem Inst Oswaldo Cruz. 1991; 86(Suppl 3):1–11. [PubMed: 1726969]

Murray PJ, Wynn TA. Protective and pathogenic functions of macrophage subsets. Nat Rev Immunol. 2011; 11:723–737. [PubMed: 21997792]

Nagaoka SI, Hassold TJ, Hunt PA. Human aneuploidy: mechanisms and new insights into an age-old problem. Nat Rev Genet. 2012; 13:493–504. [PubMed: 22705668]

Nielsen LF, Moe D, Kirkeby S, Garbarsch C. Sirius red and acid fuchsin staining mechanisms. Biotech Histochem. 1998; 73:71–77. [PubMed: 9605621]

O'Reilly S, Cant R, Ciechomska M, van Laar JM. Interleukin-6: a new therapeutic target in systemic sclerosis? Clin Transl Immunology. 2013; 2:e4. [PubMed: 25505952]

Olveda DU, Olveda RM, McManus DP, Cai P, Chau TN, Lam AK, Li Y, Harn DA, Vinluan ML, Ross AG. The chronic enteropathogenic disease schistosomiasis. Int J Infect Dis. 2014; 28:193–203. [PubMed: 25250908]

Pascual M, Fernandez-Lizarbe S, Guerri C. Role of TLR4 in ethanol effects on innate and adaptive immune responses in peritoneal macrophages. Immunol Cell Biol. 2011; 89:716–727. [PubMed: 21221123]

Porta EA. Pigments in aging: an overview. Ann N Y Acad Sci. 2002; 959:57–65. [PubMed: 11976186]

Pritchard MT, Cohen JI, Roychowdhury S, Pratt BT, Nagy LE. Early growth response-1 attenuates liver injury and promotes hepatoprotection after carbon tetrachloride exposure in mice. J Hepatol. 2010; 53:655–662. [PubMed: 20615570]

Pritchard MT, Nagy LE. Hepatic fibrosis is enhanced and accompanied by robust oval cell activation after chronic carbon tetrachloride administration to Egr-1-deficient mice. Am J Pathol. 2010; 176:2743–2752. [PubMed: 20395449]

Ramachandran P, Pellicoro A, Vernon MA, Boulter L, Aucott RL, Ali A, Hartland SN, Snowdon VK, Cappon A, Gordon-Walker TT, Williams MJ, Dunbar DR, Manning JR, van Rooijen N, Fallowfield JA, Forbes SJ, Iredale JP. Differential Ly-6C expression identifies the recruited macrophage phenotype, which orchestrates the regression of murine liver fibrosis. Proc Natl Acad Sci U S A. 2012; 109:E3186–3195. [PubMed: 23100531]

Ramm GA, Ruddell RG. Iron homeostasis, hepatocellular injury, and fibrogenesis in hemochromatosis: the role of inflammation in a noninflammatory liver disease. Semin Liver Dis. 2010; 30:271–287. [PubMed: 20665379]

Reddy GK, Enwemeka CS. A simplified method for the analysis of hydroxyproline in biological tissues. Clin Biochem. 1996; 29:225–229. [PubMed: 8740508]

Sahin H, Wasmuth HE. Chemokines in tissue fibrosis. Biochim Biophys Acta. 2013; 1832:1041–1048. [PubMed: 23159607]

Sangaralingham SJ, Wang BH, Huang L, Kumfu S, Ichiki T, Krum H, Burnett JC Jr. Cardiorenal fibrosis and dysfunction in aging: Imbalance in mediators and regulators of collagen. Peptides. 2016; 76:108–114. [PubMed: 26774586]

Schneider CA, Rasband WS, Eliceiri KW. NIH Image to ImageJ: 25 years of image analysis. Nat Methods. 2012; 9:671–675. [PubMed: 22930834]

Sobolev SM. [Result of histochemical studies on certain PAS-positive substances in macrophages]. Biull Eksp Biol Med. 1959; 47:104–109. [PubMed: 13671051]

Spandidos A, Wang X, Wang H, Dragnev S, Thurber T, Seed B. A comprehensive collection of experimentally validated primers for Polymerase Chain Reaction quantitation of murine transcript abundance. BMC Genomics. 2008; 9:633. [PubMed: 19108745]

Spandidos A, Wang X, Wang H, Seed B. PrimerBank: a resource of human and mouse PCR primer pairs for gene expression detection and quantification. Nucleic Acids Res. 2010; 38:D792–799. [PubMed: 19906719]

Street JM, Souza AC, Alvarez-Prats A, Horino T, Hu X, Yuen PS, Star RA. Automated quantification of renal fibrosis with Sirius Red and polarization contrast microscopy. Physiol Rep. 2014; 2

Stroud JS, Mutch D, Rader J, Powell M, Thaker PH, Grigsby PW. Effects of cancer treatment on ovarian function. Fertil Steril. 2009; 92:417–427. [PubMed: 18774559]

Sziksz E, Pap D, Lippai R, Beres NJ, Fekete A, Szabo AJ, Vannay A. Fibrosis Related Inflammatory Mediators: Role of the IL-10 Cytokine Family. Mediators Inflamm. 2015; 2015:764641. [PubMed: 26199463]

Tingen CM, Kiesewetter SE, Jozefik J, Thomas C, Tagler D, Shea L, Woodruff TK. A macrophage and theca cell-enriched stromal cell population influences growth and survival of immature murine follicles in vitro. Reproduction. 2011; 141:809–820. [PubMed: 21389078]

Treff NR, Krisher RL, Tao X, Garnsey H, Bohrer C, Silva E, Landis J, Taylor D, Scott RT, Woodruff TK, Duncan FE. Next Generation Sequencing-Based Comprehensive Chromosome Screening in Mouse Polar Bodies, Oocytes, and Embryos. Biol Reprod. 2016; 94:76. [PubMed: 26911429]

Uri-Belapolsky S, Shaish A, Eliyahu E, Grossman H, Levi M, Chuderland D, Ninio-Many L, Hasky N, Shashar D, Almog T, Kandel-Kfir M, Harats D, Shalgi R, Kamari Y. Interleukin-1 deficiency prolongs ovarian lifespan in mice. Proc Natl Acad Sci U S A. 2014; 111:12492–12497. [PubMed: 25114230]

Ushiki T. Collagen fibers, reticular fibers and elastic fibers. A comprehensive understanding from a morphological viewpoint. Arch Histol Cytol. 2002; 65:109–126. [PubMed: 12164335]

Vogel B, Siebert H, Hofmann U, Frantz S. Determination of collagen content within picrosirius red stained paraffin-embedded tissue sections using fluorescence microscopy. MethodsX. 2015; 2:124–134. [PubMed: 26150980]

Wang X, Seed B. A PCR primer bank for quantitative gene expression analysis. Nucleic Acids Res. 2003; 31:e154. [PubMed: 14654707]

Weber LW, Boll M, Stampfl A. Hepatotoxicity and mechanism of action of haloalkanes: carbon tetrachloride as a toxicological model. Crit Rev Toxicol. 2003; 33:105–136. [PubMed: 12708612]

Whittaker P, Kloner RA, Boughner DR, Pickering JG. Quantitative assessment of myocardial collagen with picrosirius red staining and circularly polarized light. Basic Res Cardiol. 1994; 89:397–410. [PubMed: 7535519]

Wick G, Grundtman C, Mayerl C, Wimpissinger TF, Feichtinger J, Zelger B, Sgonc R, Wolfram D. The immunology of fibrosis. Annu Rev Immunol. 2013; 31:107–135. [PubMed: 23516981]

Wood CD, Vijayvergia M, Miller FH, Carroll T, Fasanati C, Shea LD, Brinson LC, Woodruff TK. Multi-modal magnetic resonance elastography for noninvasive assessment of ovarian tissue rigidity in vivo. Acta Biomater. 2015; 13:295–300. [PubMed: 25463483]

Wu R, Van der Hoek KH, Ryan NK, Norman RJ, Robker RL. Macrophage contributions to ovarian function. Hum Reprod Update. 2004; 10:119–133. [PubMed: 15073142]

Wynn TA, Barron L. Macrophages: master regulators of inflammation and fibrosis. Semin Liver Dis. 2010; 30:245–257. [PubMed: 20665377]

Wynn TA, Ramalingam TR. Mechanisms of fibrosis: therapeutic translation for fibrotic disease. Nat Med. 2012; 18:1028–1040. [PubMed: 22772564]

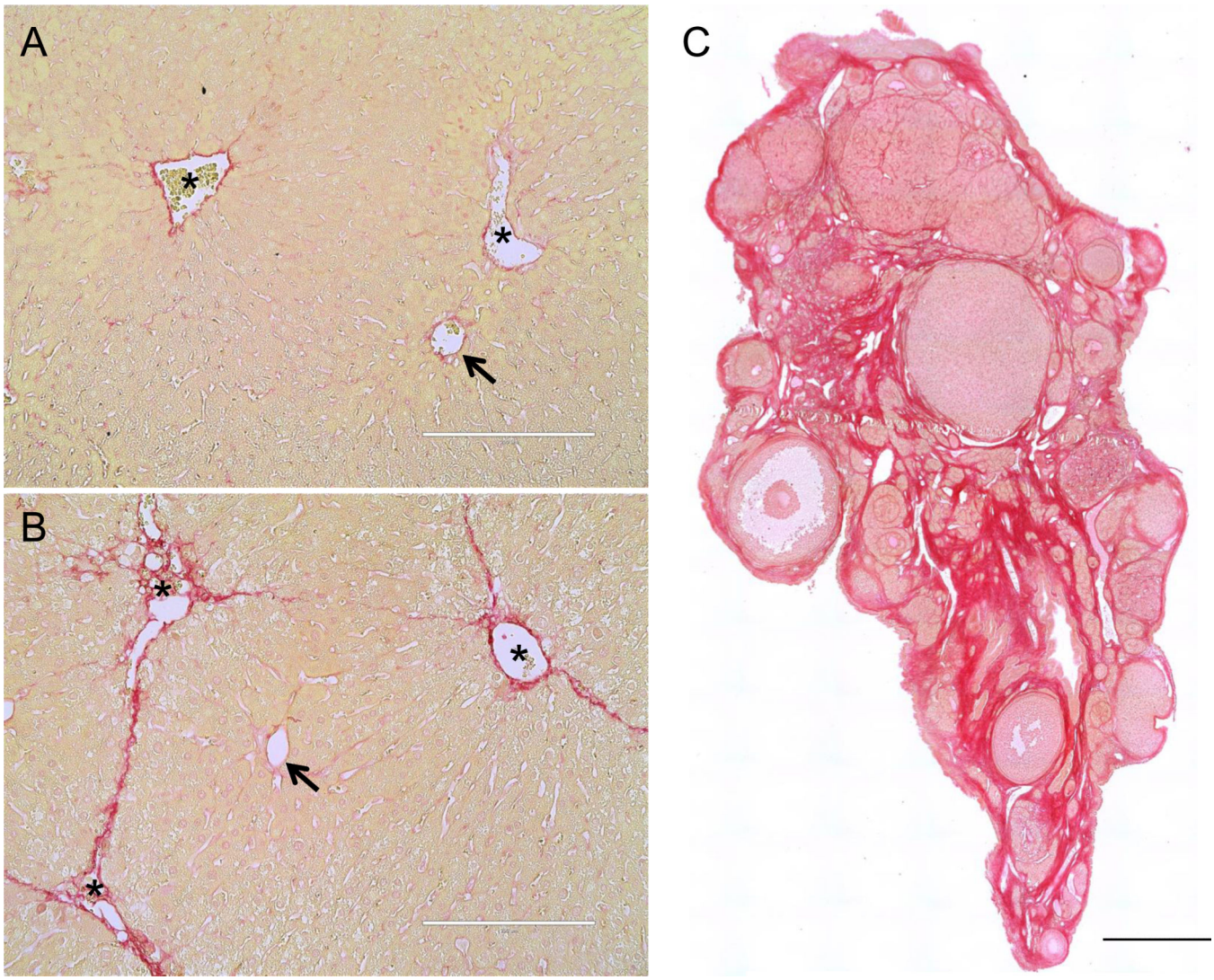

Figure 1. Picrosirius Red staining detects fibrosis

Liver tissue sections from (A) a control mouse injected with vehicle and (B) a mouse injected chronically with CCl_4 (2 times per week for 5 weeks). Arrows highlight the hepatic vessels in the periportal areas and asterisks highlight the central vein. (C) An ovarian tissue section from a 21-month old CD1 mouse was stained with PSR using the same protocol. The intense red staining corresponds to fibrotic regions. The scale bars in (A) and (B) are 200 μm and 0.4 mm in (C).

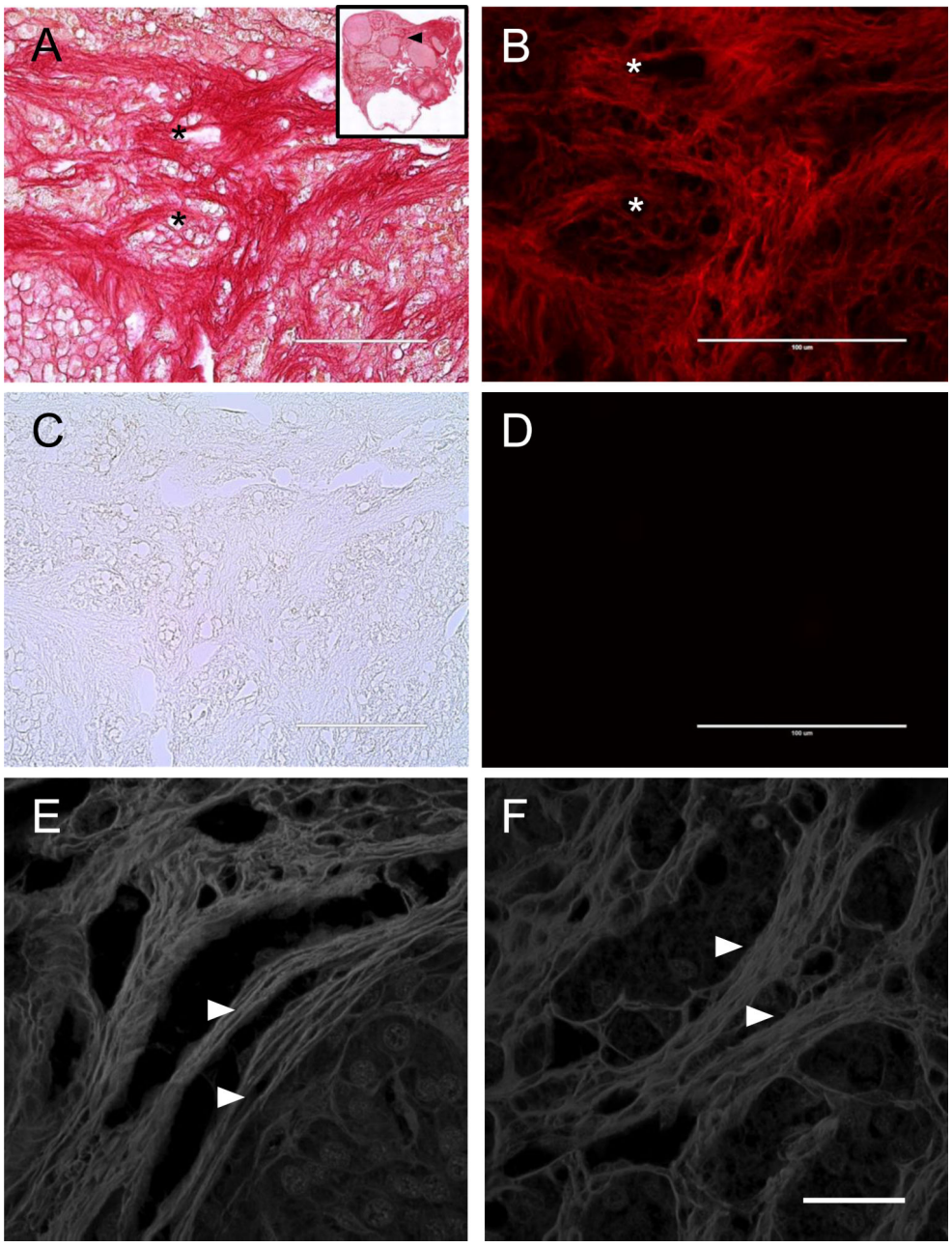

Figure 2. Picrosirius Red staining exhibits red fluorescence and shows fibrils organized into bundles within the ovarian stroma

PSR-stained ovarian tissue from a 22-month old CD1 mouse visualized by (A) brightfield microscopy and (B) epifluorescence microscopy using a Texas Red LED Light Cube. The inset in (A) shows the entire ovarian section, with the region examined in (A-D) marked by a black arrowhead. An adjacent unstained section was imaged with the same settings by (C) brightfield and (D) epifluorescence microscopy. The asterisks mark corresponding regions between brightfield and fluorescence images. The scale bars are 100 μm. (E, F) PSR stained ovarian tissue sections from 21- and 22-month old CD1 mice imaged by confocal microscopy using a 532 nm laser. The white arrowheads highlight fibrils that are organized

into larger bundles. Maximum projections of 0.4 μm-thick optical sections are shown. The scale bar is 25 μm.

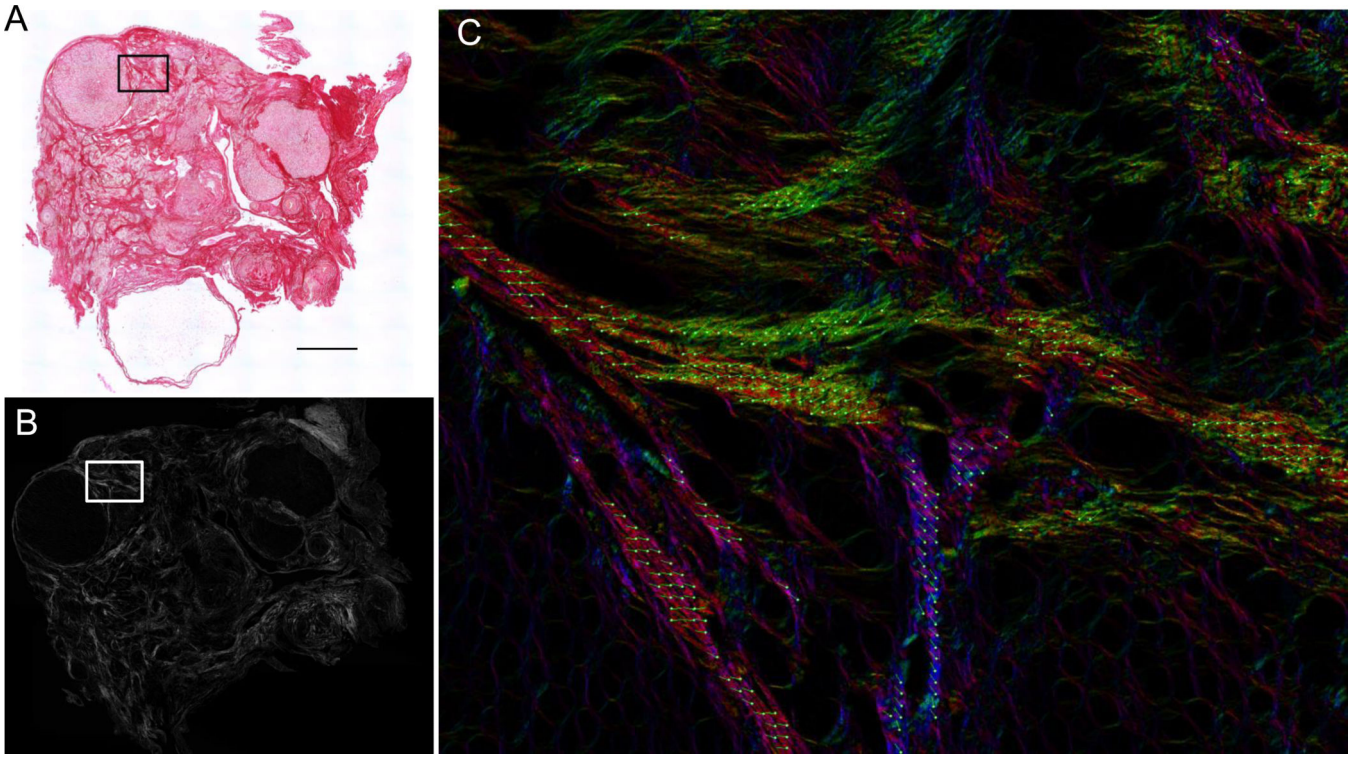

Figure 3. Picrosirius Red fibers in the aged ovary are birefringent

A PSR-stained ovarian tissue section from a 22-month old CD1 mouse visualized by both (A) brightfield microscopy and (B, C) circularly polarized light microscopy (Abrio LCPolScope). The boxed region in (A, B) is magnified in (C) where the false color image with retardance vectors (green lines) reflects the orientation of the co-aligned fibers. The scale bar is 0.4 mm.

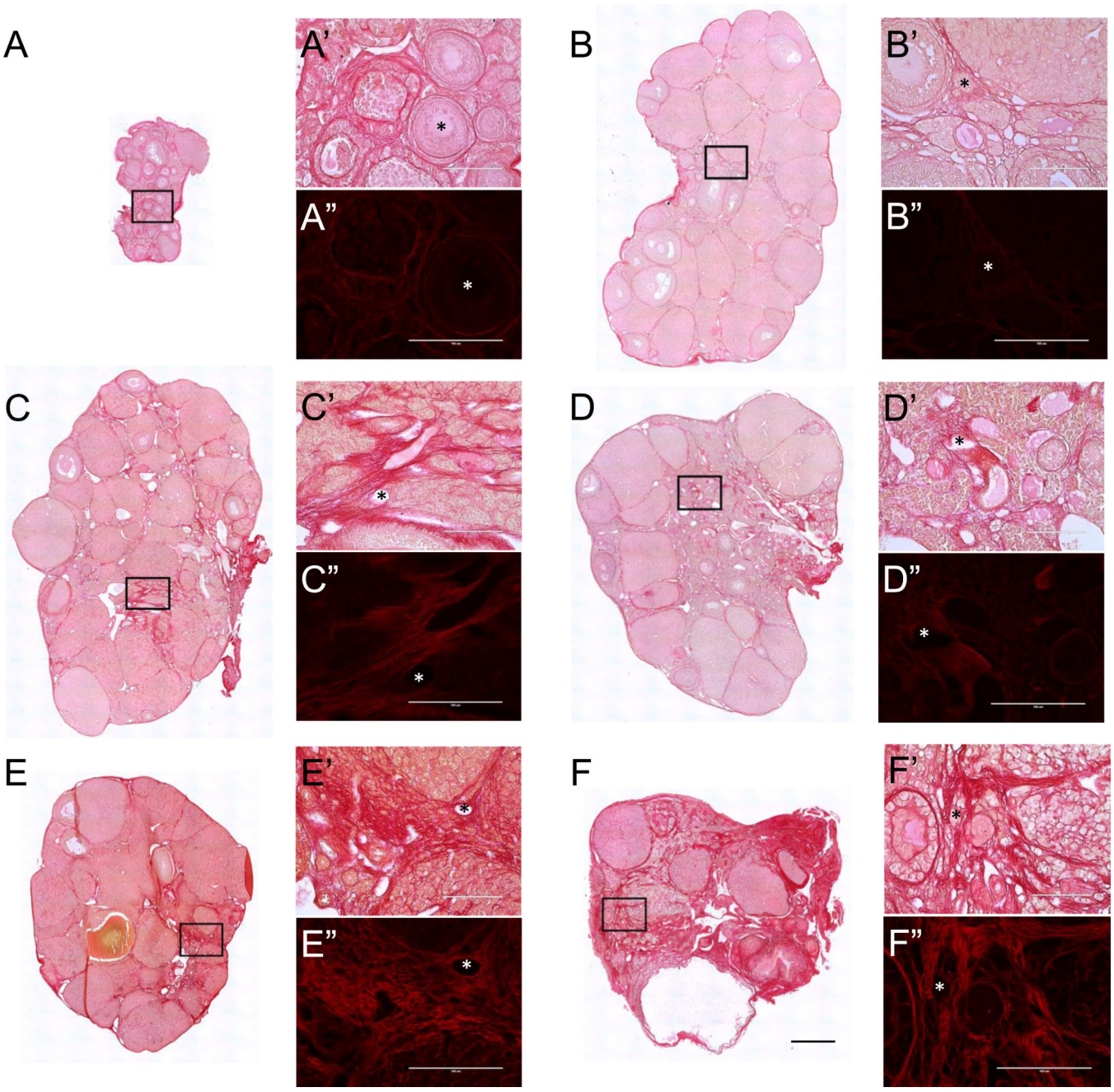

Figure 4. PSR staining expands throughout the ovarian stroma with advanced reproductive age

Scans of PSR-stained ovarian sections from (A) 6-week old, (B) 5-month old, (C) 7-month old, (D) 9-month old (E) 18-month old, and (F) 22-month old CD1 mice visualized by brightfield microscopy. The scale bar for images in (A-F) is 0.4 mm. (A'-F' and A"-F") are higher magnification images from the specific regions of the ovarian stroma that are boxed in (A-F). Brightfield images are shown in (A'-F') and fluorescence images are shown in (A"-F"). The fluorescence images were taken using a Texas Red LED Light cube with constant settings that were established for the 22-month old sample (F"). Therefore intensity

differences across ages can be compared. Asterisks mark corresponding regions between brightfield and fluorescence images. Scale bars in (A'-F' and A"-F") are 100 μm.

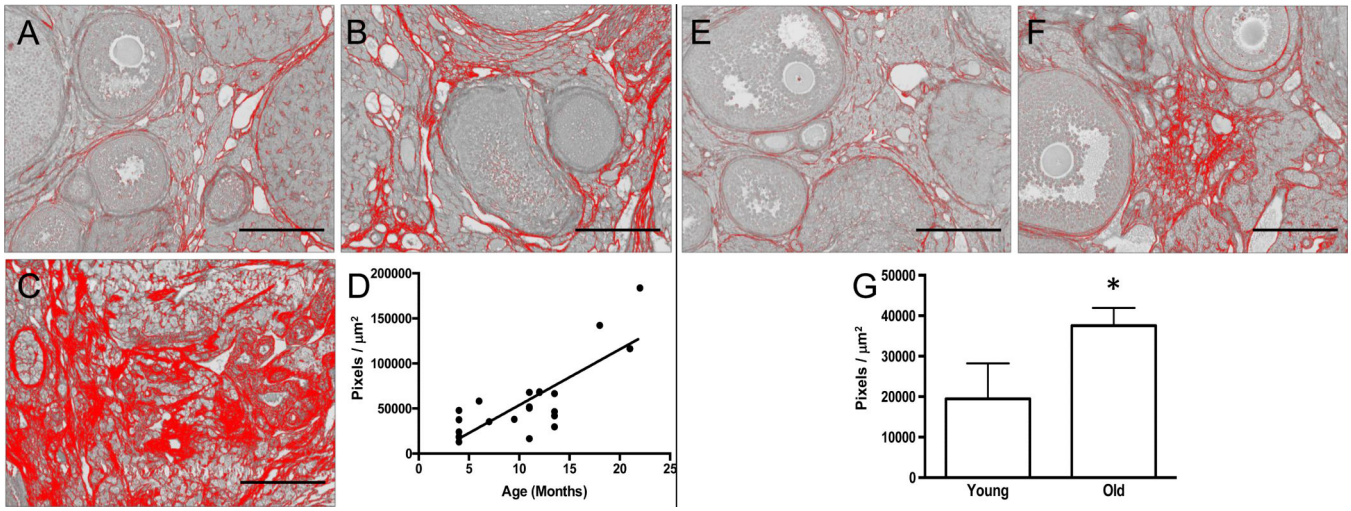

Figure 5. Fibrosis significantly increases in the ovarian stroma with advanced reproductive age in both CD1 and CB6F1 mice

Representative processed color threshold images of PSR-stained ovarian tissue sections used to quantify fibrosis from CD1 mice that were (A) 4-months old, (B) 13.5-months old, and (C) 22-months old. (D) Graph showing the relationship between CD1 mouse age (months) and the average area of PSR-positive staining per ovarian section (pixels/µm^2). A significant linear relationship exists between these variables (Pearson's correlation, $P < 0.0001$ and $R^2 = 0.6413$). Representative processed color threshold images of PSR-stained ovarian tissue sections used to quantify fibrosis from CB6F1 mice that were (E) 6-12 weeks old (young) and (F) 14-17 months old (old). (G) Graph comparing the average area of PSR-positive staining per ovarian section (pixels/µm^2) between reproductively young and old CB6F1 mice. The asterisk indicates a significant difference ($P = 0.03$). In all images, the red corresponds to PSR-positive staining, and scale bars are 200 µm.

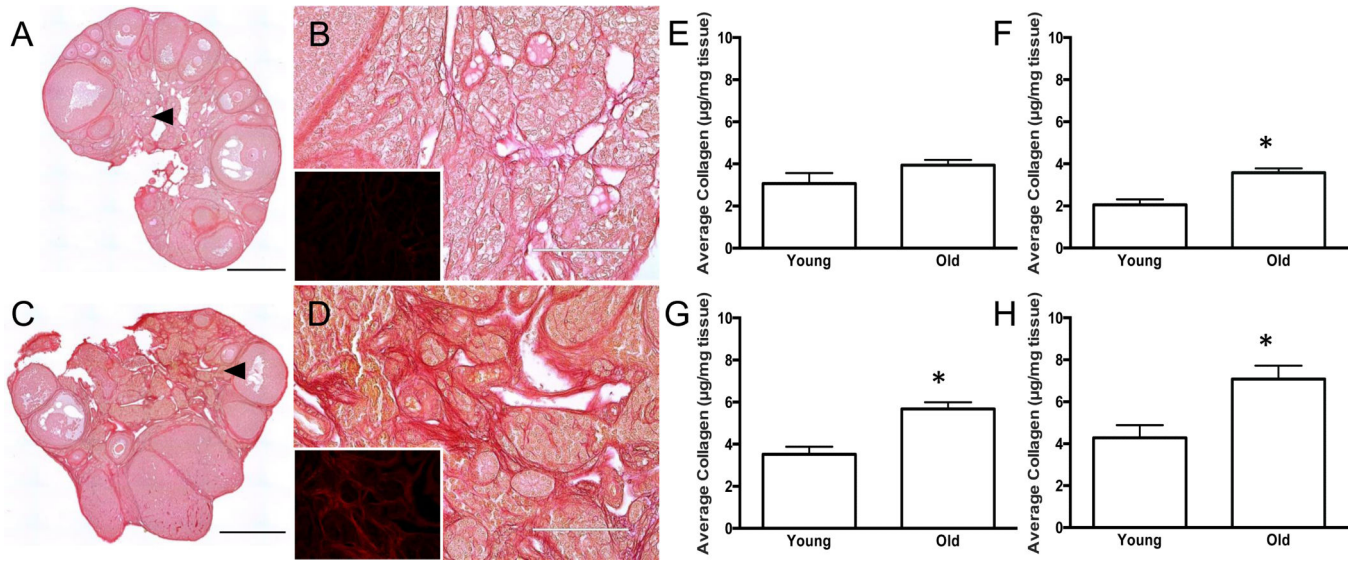

Figure 6. Reproductive-age associated increases in PSR staining correlate with increased ovarian hydroxyproline content

Scans of PSR-stained ovarian sections from (A, B) 6-12 week old (young) and (C, D) 14-17 month old (old) CB6F1 mice visualized by brightfield microscopy. Regions highlighted by the arrowheads in (A, C) are further magnified in (B, D). The insets in (B, D) show the corresponding fluorescence that is apparent when the PSR-stained tissue is viewed using epifluorescence with a Texas Red LED Light Cube. The fluorescence images were taken using constant settings that were established for the old ovary sample (D, inset), and therefore, intensity differences between the age cohorts can be compared. Scale bars are 0.4 mm in (A, C) and 100 µm in (B, D). (E-H) Extrapolation of collagen content (µg/mg tissue) from hydroxyproline quantification in ovaries from reproductively young and old CB6F1 mice. Each graph represents data from a single trial. Asterisks mark significant differences (E: P = 0.255; F: P = 0.044; G: P = 0.004; H: P = 0.0186).

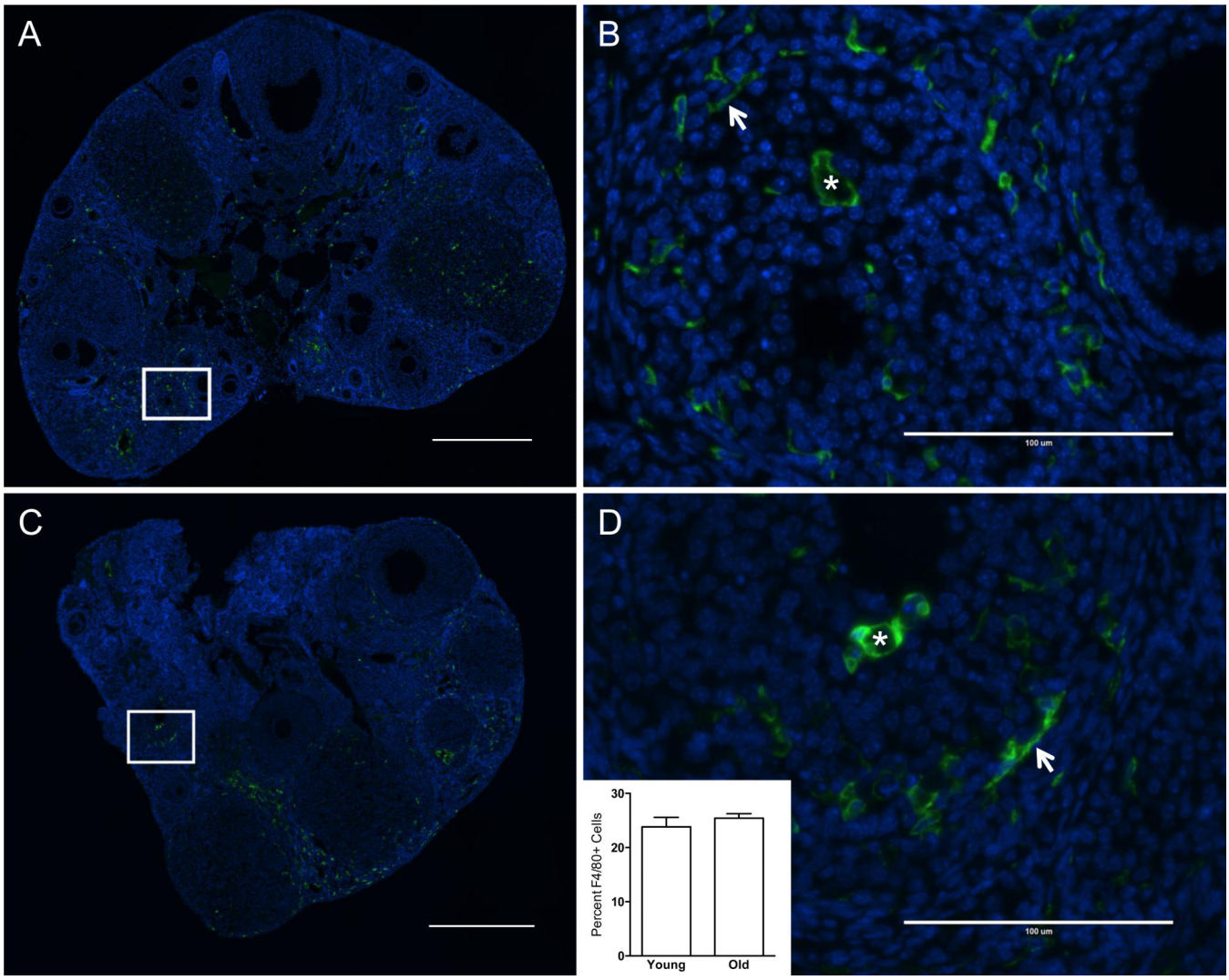

Figure 7. F4/80-positive macrophages are present in the ovarian stroma irrespective of reproductive age

Representative immunofluorescence images of ovarian sections from reproductively (A, B) young and (C, D) old CB6F1 mice stained with an F4/80-specific antibody. F4/80-positive cells are green and nuclei stained with DAPI are blue. Boxed regions in scans of entire ovarian sections (A, C) are further magnified in (B) and (D). Arrows highlight spindle shaped macrophages whereas asterisks highlight ovoid macrophages that have F4/80-positive staining around the entire cell surface. The inset in (D) shows the percentage of F4/80-positive cells relative to total cell number in ovarian sections from reproductively young and old mice (P = 0.45). Scale bars are 0.4 mm in (A, C) and 100 μm in (B, D).

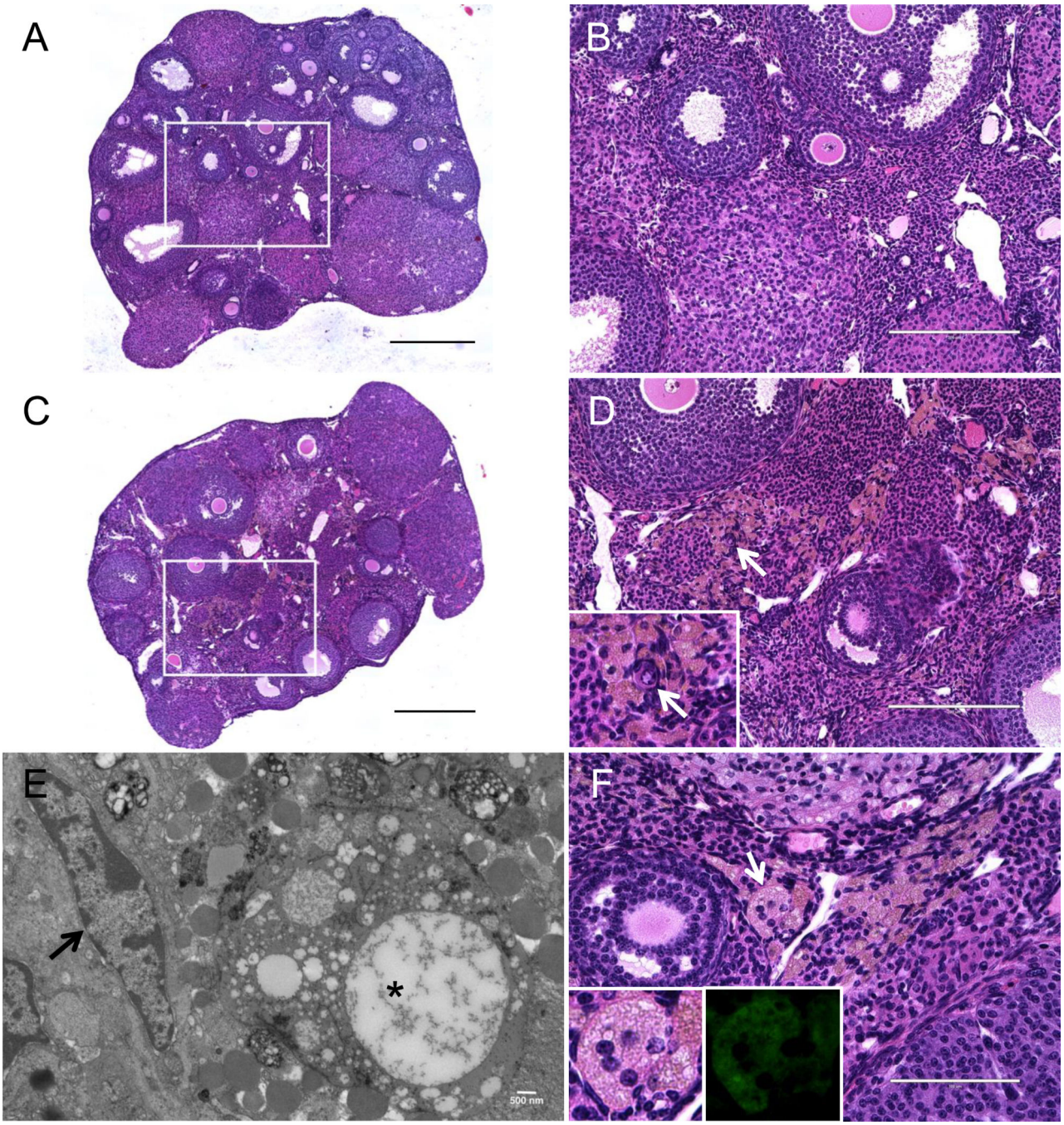

Figure 8. Multinucleated giant cells are present within the ovarian stroma of reproductively old mice

Hematoxylin and Eosin (H&E) staining was performed on ovarian sections from (A, B) 6-12 week old (young) and (C, D, F) 14-17 month old (old) CB6F1 mice. (A) and (C) are scans of the entire ovarian sections, and boxed regions are further magnified in (B) and (D) to highlight the ovarian stroma. In (C, D, F), multinucleated giant cells appear foamy and stain brown by H&E. The white arrows in (D) highlight a primordial follicle (inset) that localizes within this microenvironment containing multinucleated giant cells. (E) An electron micrograph of a thin ovarian tissue section from a reproductively old animal. The black

arrow highlights a fibroblast with an elongated nucleus, and the asterisks highlights an enlarged giant cell with vacuoles and inclusion bodies. Another representative image of the ovarian stroma from reproductively old CB6F1 mice is shown in (F). The white arrow highlights a particular multinucleated giant cell in which 5 nuclei are clearly visible. This cell is magnified in the inset and its autofluorescent properties are shown (inset, right). Scale bars in (A, C) are 0.4 mm, in (B, D) are 200 μm, 500 nm in (E), and 100 μm in (F).

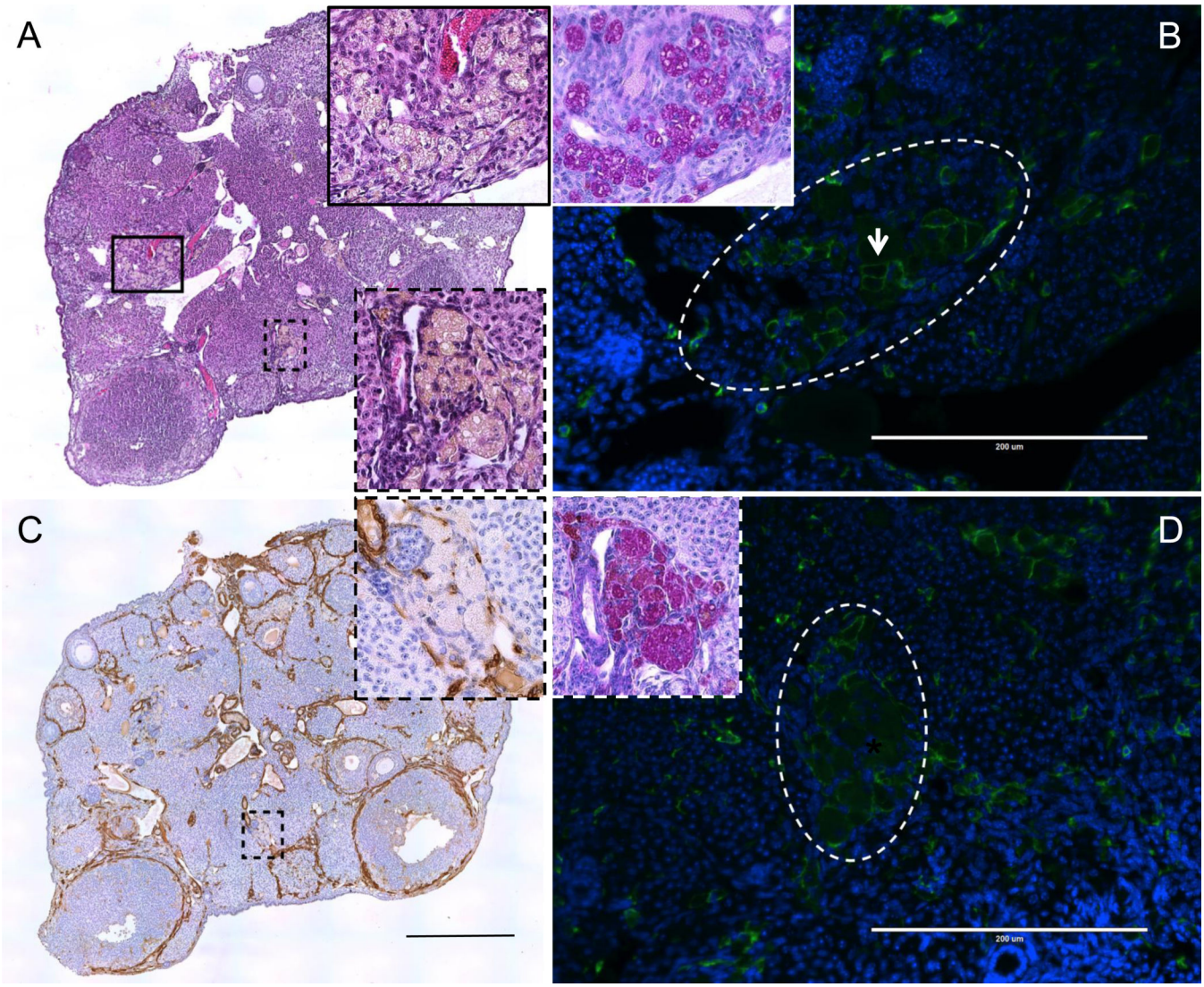

Figure 9. Multinucleated giant cells in the ovarian stroma are fused macrophages

(A) A representative Hematoxylin and Eosin (H&E) stained ovarian section from a reproductively old CB6F1 mouse. The boxed regions (black solid and dashed), which highlight clusters of multinucleated giant cells, are further magnified in the insets. The black solid and dashed boxed regions are further examined in (B) and (C, D), respectively. In (B, D), ovarian sections were stained with an F4/80 antibody (green) and nuclei were visualized by DAPI (blue). The multinucleated giant cell clusters visible by H&E in (A, C) are encircled by the white dashed lines in (B, D). The arrow in (B) highlights cells individual cells expressing F4/80 at the cell periphery in contrast to fused cells that lack complete borders (D). Insets in (B, D) show Periodic Acid Schiff (pink) staining within the clusters of multinucleated giant cells. Nuclei were visualized with hematoxylin (blue). In (C) an ovarian section was stained with an α-Smooth Muscle Actin antibody (brown) and nuclei were visualized with hematoxylin (blue). The inset highlights the multinucleated giant cell cluster within the black dashed boxed region. Images in (A) and (C) are scans of the entire ovarian sections, whereas all other images highlight specific regions of interest in the ovarian

stroma. All staining was done on sections that were between 5-30 μm of each other to ensure that the same clusters of multinucleated giant cells was examined. The scales bars in (A, C) are 0.4 mm and in (B, D) are 200 μm.

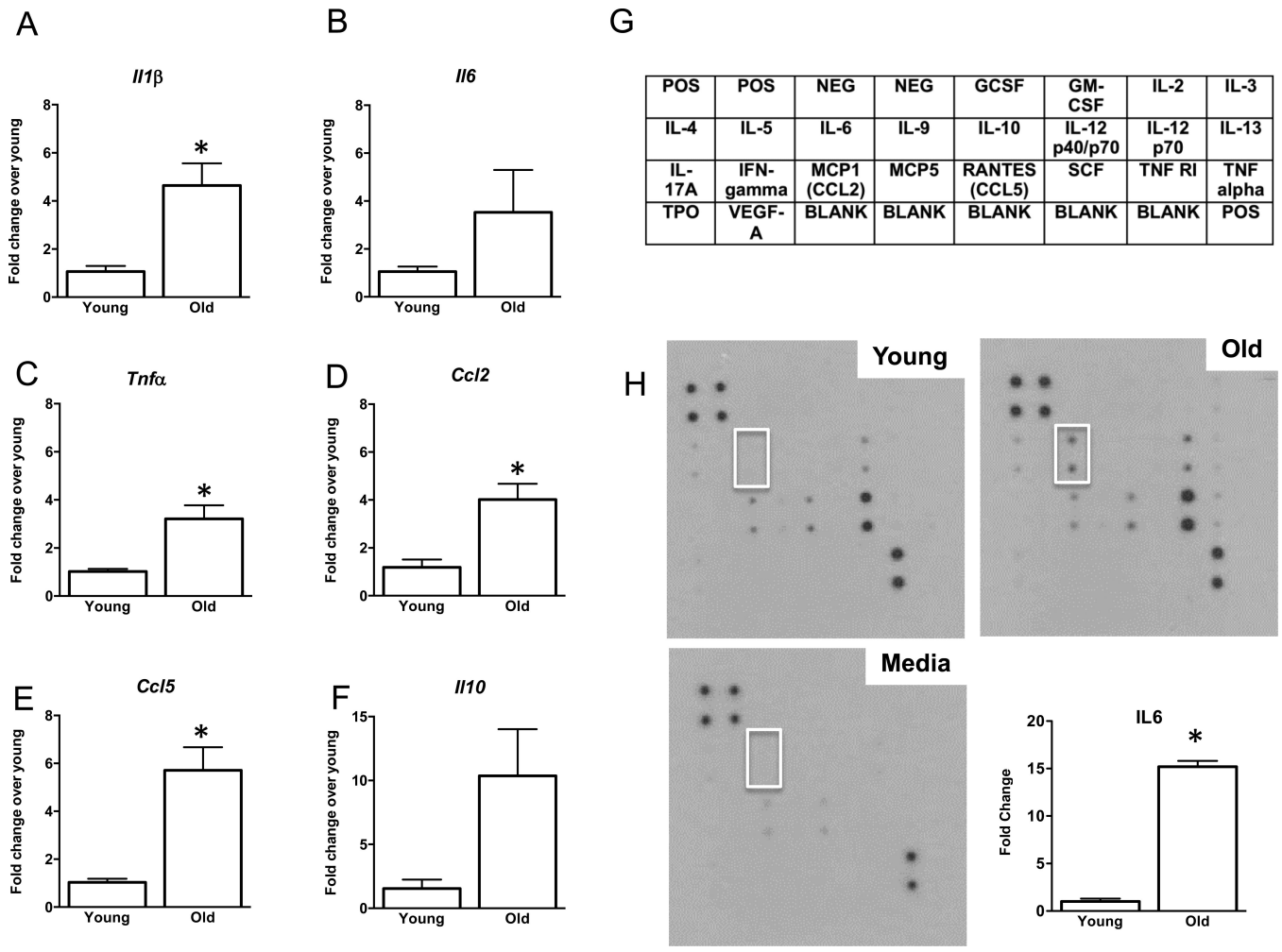

Figure 10. Reproductive aging is associated with an inflammatory ovarian microenvironment

Relative gene expression levels of (A) *Il1b* (B) *Il6* (C) *Ccl2* (D) *Tnfa* (E) *Ccl5,* and (F) *Il10* in ovaries from 6-12 week old (young) and (14-17 month old (old) CB6F1 mice. The data is shown as fold change expression in ovaries from reproductively old mice compared to reproductively young mice. Asterisks indicate significant differences (A: P = 0.002 ΔCt, P = 0.009 fold change; B: P = 0.07 ΔCt, P = 0.15 fold change; C: P = 0.02 ΔCt, P = 0.008 fold change; D: P = 0.002 ΔCt, P = 0.008 fold change; E: P = 0.0002 ΔCt, P = 0.003 fold change; F: P = 0.02 ΔCt, P = 0.054 fold change). (G) Schematic of the cytokines interrogated on the RayBio C-Series Mouse Cytokine Antibody Array C1. Antibodies in each column are printed in duplicate. (H) Representative arrays probed with spent culture media from ovaries from reproductively young (top left) and old (top right) mice and control media only (bottom left). The white box highlights the spots on the arrays that correspond to IL-6. The relative expression of IL-6 in the conditioned culture media from ovaries isolated from reproductively young and old mice was quantified (bottom right), and the asterisks indicates a significant difference (P = 0.0024)

Table I

Penetrance of macrophage giant cells in the ovarian stroma

Age Cohorts	# of mice with macrophage giant cells/total (%)
CD1 Mice	
4 – 7 months	0/8 (0%)
10 – 14 months	7/10 (70%)
18 – 22 months	3/3 (100%)
CB6F1 Mice	
6 – 12 weeks (young)	0/10 (0%)
14 - 17 months (old)	8/8 (100%)